An Induced Seismicity Non-Ergodic Ground Motion Prediction Equation (GMPE) in the Oklahoma Region

Final Technical Report Submitted to the U.S. Geological Survey
NEHRP Grant **G18AP00076**
Award Period August 2018 to August 2019

Prepared By:

Melanie Walling[1]
[1]GeoEngineers, Inc.
17425 NE Union Hill Road Ste 250
Redmond, WA 98052
mwalling@geoengineers.com

Nicolas Kuehn[2]
[2]Natural Hazards Risk and Resiliency Research Center (NHR3),
University of California, Los Angeles
Los Angeles, CA 90095
kuehn@ucla.edu

Norman Abrahamson[3]
[3]455 Davis Hall
University of California, Berkeley
Berkeley, CA 94720
abrahamson@berkeley.edu

November 5, 2021

Abstract

We have developed a non-ergodic ground motion model (GMM) that explicitly models systematic source, path, and site effects the Oklahoma region using the 2018 BC Hydro Flatfile for potentially induced earthquakes (PIE). PIE events are attractive to develop a non-ergodic GMM. Due to the high rate of occurrence of induced earthquakes, PIE datasets have a significant number of recordings at sites from sources at similar locations.

The median prediction of our non-ergodic GMM is modeled as a base ergodic GMM and a non-ergodic adjustment. The base ergodic GMM is the ASK21 GMM adjusted for regional differences between Oklahoma and California ground motion. The non-ergodic adjustment is comprised of two components. The anelastic attenuation term as cell-specific attenuation terms, which is the sum over the attenuation from small cells, and the systematic event terms as spatially varying systematic event terms.

The model parameters are estimate using an integrated nested Laplace (INLA) approximation that deterministic Bayesian inference method which approximates posterior marginal distributions. The model INLA approximation is performed with the `R-INLA` package. For spatial models, `R-INLA` implements the *stochastic partial differential equations* (SPDE) approach, which allows for fast inference of Bayesian spatial models.

The model is estimated on 113,625 ground motions from 362 well-recorded events. In total, apart from the random effects there were 10 parameters to estimate: 4 fixed effects (the intercept, the Moho bounce adjustment, the linear site scaling adjustment, the linear R-term), and six hyperparameters (ϕ_0, τ_0, $\phi_{S2S,0}$, the range and standard deviation of the systematic event constants, and the standard deviation of the cell-specific attenuation terms). The final GMM is applicable to PIE events occurring within the Oklahoma region at distances less than 300 km from the site and for spectral periods less than or equal to 1.5 secs.

1 Introduction

Ground-motion models (GMMs) develop estimates of peak ground-motion and response spectral amplitudes as a function of source, path and site parameters and are an important input into a seismic hazard assessment. A classical approach for developing GMMs is to use ground-motion

recordings of earthquake events that occurred in similar tectonic regions as the input data to a regression analysis performed in the model development process. The prevailing assumption in this approach is that average site-, path- and source-effects displayed in the data is equivalent to unique site-, path-, and source-effects at discrete sites and earthquake scenarios (Anderson and Brune, 1999). This assumption is referred to as the ergodic assumption.

GMMs developed under the ergodic assumption ignore systematic, repeatable, location-specific source, path and site effects. Instead, these GMMs average over these effects, which increases the value of the aleatory variability because the unmodeled systematic effects are treated as random variability that applies to all sites.

In the last two decades, there has been a significant increase in the volume of collected ground-motion recordings due to an increase in strong-motion instrumentation deployment. With large datasets more that have multiple recordings at individual stations and events, the ground-motion field is starting to pivot away from a strict adherence to ergodic assumption towards a relaxation of it. A first step in this regard is the inclusion of systematic site effects in a GMM, which can be estimated from multiple recordings at a single site. This leads to a decrease in the value of the within-event standard deviation, and is referred to as *single-station sigma* (Atkinson, 2006; Rodriguez-Marek et al., 2011, 2014). A further step beyond this is to introduce terms that can be different for some broad geographical regions (Stafford, 2014) to allow for differences in anelastic attenuation or linear site scaling between regions.

A methodology for a full relaxation of the ergodic assumption in GMM has been proposed in Landwehr et al. (2016) who developed a fully non-ergodic GMM for California based on a spatially varying coefficient model (SVCM, Bussas et al., 2017; Gelfand et al., 2003). In an SVCM, the coefficients vary as a continuous function of location, thus encoding spatial effects on ground motion. The model of Landwehr et al. (2016) is formulated as a Bayesian hierarchical model, where the spatially varying terms are modeled as adjustment terms with a Gaussian process (GP) prior.

Another approach to model spatial varying effects is described in Dawood and Rodriguez-Marek (2013) who proposed a model to account for path effects, where the anelastic attenuation term in a GMM is modeled as a sum over the attenuation from small cells. This cell-specific

attenuation model was extended by Kuehn et al. (2019), who cast the cell-specific attenuation coefficients as random effects in a Bayesian model to account for their uncertainty. Abrahamson et al. (2019) combined the models of Landwehr et al. (2016) and Kuehn et al. (2019) to perform a non-ergodic PSHA for three sites in California.

In the work presented here, we apply the method of Kuehn et al. (2019) and Dawood and Rodriguez-Marek (2013) to develop a partially non-ergodic GMM of potentially induced earthquake (PIE) ground motion for the Oklahoma region.

l

2 Model Fitting

The model fitting was performed using a Bayesian inference approach using the package `R-INLA`[1] (Bakka et al., 2018; Bivand et al., 2015; Lindgren and Rue, 2015; Rue et al., 2017) for the computer environment `R` (R Core Team, 2021). `R-INLA` implements the *integrated nested Laplace approximation* (INLA, Rue et al., 2009), which is a deterministic Bayesian inference method which approximates posterior marginal distributions (Martino and Riebler, 2020). INLA has been widely used for estimation of large-scale spatial and spatio-temporal models, for example in ecology (Bachl et al., 2019; Lezama-Ochoa et al., 2020; Vilela et al., 2021) or disease modeling (e.g. Moraga, 2019; Schrödle and Held, 2011). It has also been used to model spatially varying seismicity (Bayliss et al., 2020; D'Angelo et al., 2020), evaluate the spatial damage distribution of earthquake (Wilson, 2020), and in seismic tomography (Zhang et al., 2016). For an application of INLA to the development of non-ergodic GMMs, see Kuehn (2021a,c).

For spatial models, `R-INLA` implements the *stochastic partial differential equations* (SPDE) approach (Bakka et al., 2018; Lindgren et al., 2011), which allows for fast inference of Bayesian spatial models. In the SPDE approach, the Gaussian field is approximated by a basis function approximation (Lindgren et al., 2011), which makes the precision matrix (the inverse of the covariance matrix) sparse. This is a desirable feature because it can be exploited numerically

[1] www.r-inla.org

(Simpson et al., 2012). The basis functions are then evaluated on a Constained Refined Delaunay Triangular (CRDT) mesh over the study region, which then maps spatial effects to the mesh nodes.

For introductory texts on INLA, see e.g. Gómez-Rubio (2020); Krainski et al. (2019)[2]. Franco-Villoria et al. (2019) provide a comprehensive overview of INLA in the context of VCMs. For a brief introduction to INLA in the context of GMM development, see Kuehn (2021b).

3 PIE Ground Motion

PIE refers to earthquakes that are caused by human activity that alters the stresses and strains of the shallow crust. PIE are generally small to moderate magnitude events that occur at shallower depths than tectonic events. Atkinson and Assatourians (2017) compared the PIE ground motion to tectonic GMMs and found that several GMMs (Abrahamson et al., 2014; Atkinson and Assatourians, 2015; Yenier and Atkinson, 2015) are appropriate in functional form and overall amplitude scaling for **M** 3.5-6 at distances up to 50 km when a smaller depth to top-of-rupture is prescribed, suggesting that ground motion shaking from induced events scales similar to the shaking from natural tectonic events when the depth to rupture is accommodated.

PIE events are attractive to develop a non-ergodic GMM. Due to the high rate of occurrence of induced earthquakes, PIE datasets have a significant number of recordings at sites from sources at similar locations. On the surface this makes them ideal for modeling repeatable source, path and site effects in a non-ergodic GMM. As we discovered during the modeling process, having such a large dataset to work with lead to challenges at times: evaluation of the data quality of the meta data and the ground-motion data for a large number of recordings is difficult; long calculation times are required for the large number of recordings.

[2] https://becarioprecario.bitbucket.io/spde-gitbook/index.html and https://becarioprecario.bitbucket.io/inla-gitbook/index.html

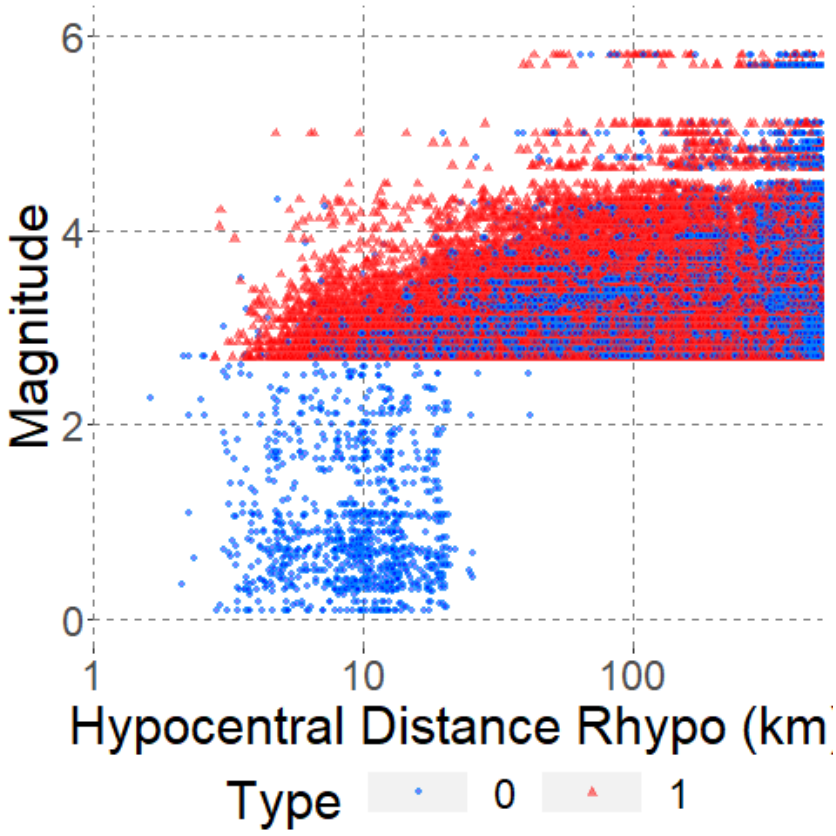

Figure 1: Original Dataset

4 PIE DataSet

The PIE dataset we used is a filtered version of the 2018 BC Hydro Flatfile for PIE ground motion (Gregor, 2018) which was compiled from the (Mahani and Kao) and Rennolet et al. (2018) databases. The Mahani and Kao database was compiled from PIE events located in the Montney Play region of northeastern British Columbia, while the Rennolet et al. (2018) database was compiled from PIE events in the Oklahoma and Kansas region of the United States. The PIE 2018 BC Hydro Flatfile is a total of 175,850 records collected between the time periods of January 2009 and December 2016. A plot showing the distribution of the earthquake magnitude over hypocentral distance represented in the 2018 BC Hydro Flatfile is shown in Figure 1.

In this study, only the Rennolet et al. (2018) database was relevant. Advantageously, the Rennolet et al. (2018) database represents the majority records in the 2018 BC Hydro PIE Flatfile, making up 174,787 records out of a total of 175,850 records collected between the time periods of January 2009 and December 2016. The recordings represent 3771 PIE events of

magnitudes greater than 3 and distances less than 500 km, at 531 stations. Processed time histories ground motions were computed in RotD50 and RotD100 (Boore, 2010) acceleration response spectra for a spectral damping of 5% for PGA, PGV, and a suite of 80 spectral periods between 0.1 and 10 seconds. The 2018 BC Hydro PIE Flatfile retained RotD50 values, which are approximately equal to the geomean values from the two horizontal components that the Mahani and Kao (2018) data are based on. Please refer to Gregor (2018) further description of the 2018 BC Hydro Flatfile.

Our final database filtered out undesirable records from the parent flatfile. A total of 4,165 records were removed for apparent gain problems. This included included the entire RH** array, CSTR station, and the PW** array. Stations that had the same location but different station identification labels were removed: OK026, OKCFA, W41A, W41B, ARK2, ARK3, MA01, MA07, 237A, 237B, Z35A, Z35B, U38A, U38B, Z38A, Z35B, T35A, T35B, S39A, S39B, R32A, R32B, R40A, R40B, OK028 and CHOK. Many of these stations shared the same $Vs30$, but a few did not. This removed 22,931 records. Station and events having locations outside Oklahoma/Kansas region were also filtered out; this removed an additional 39,573 recordings. Stations having large station terms from a simple regression sensitivity were filtered out: stations FW07, FNO, W35A, FW11, IFCF, and IFDF. This removed an additional 3,389 recordings. Finally, individual records flagged as outliers being more than 4 standard deviations from the results of a simple linear regression were filtered out; this removed an additional 785 recordings. The final filtered dataset consisted of 113,625 of records and is shown in Figure 2.

A key issue for using this data set is the estimation of the moment magnitude for the smaller events. As noted by Abrahamson et al. (2021), there is a systematic difference between the ground motions from earthquakes with direct estimates of the moment magnitude (set 1) as compared to the residuals from earthquakes in which the moment magnitude is estimated using a conversion from a different magnitude scale (set 2). The direct moment estimates lead to ground motions that are about a factor of 2 larger than the converted magnitudes. This corresponds to about a 0.25 difference in the magnitudes.

This magnitude conversion issue has not been resolved yet. In Abrahamson et al. (2021),

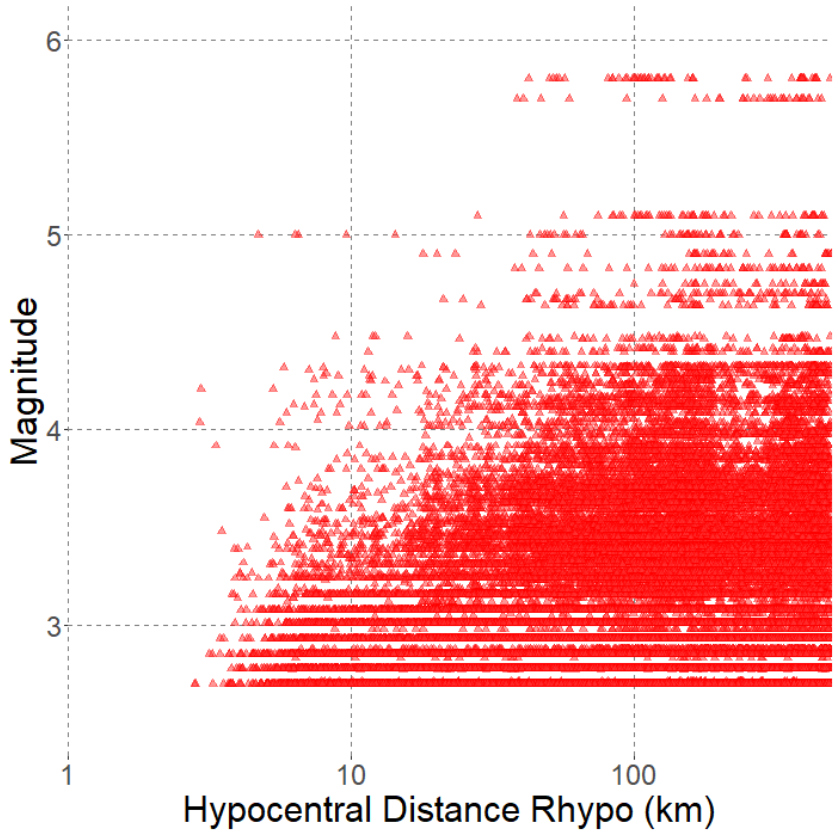

Figure 2: Filtered Dataset

the same data set was used to develop modifications to three of the NGA-W2 GMMs to be applicable to small magnitude events at short distances. Different approaches were used to address the magnitude conversion for the modifications to the three GMMs: the modification of the CB14 GMM included both set 1 and set 2 data; the modification of the CY14 GMM only included the set 1 data; the modification of the ASK14 GMM included both set 1 and set 2 data but with a modification to the small magnitudes of +0.05 for set 1 and -0.25 for set 2.

In this study, we included the data from both sets 1 and 2 with their reported magnitudes, consistent with the approach used by Abrahamson et al. (2021) for the modification to the CB14 GMM. Magnitude errors are mapped into the source terms. If there two sets of events sample the same regions, then the effect of magnitude errors will be to increase the between-event standard deviation, but if there two sets of events are clustered spatially, then the magnitude errors will affect the non-ergodic source terms.

5 non-ergodic Ground-Motion Model

A non-ergodic GMM is a model that explicitly models systematic source, path, and site effects. Hence, the prediction of the GMM becomes dependent on the source and site location. Typically, the median prediction of a non-ergodic GMM is modeled as a base model, which does not depend on location, plus location specific source, path, and site effects

$$\mu_{nonerg}(\vec{\xi}, \vec{x}_e, \vec{x}_s) = \mu_{base}(\vec{\xi}) + \delta L(\vec{x}_s) + \delta P(\vec{x}_s, \vec{x}_s) + \delta S(\vec{x}_s) \tag{1}$$

where $\delta L(\vec{x}_s)$, $\delta P(\vec{x}_s, \vec{x}_s)$, $\delta S(\vec{x}_s)$ are systematic source, path, and site effects, $\vec{\xi}$ is a vector of predictor variables describing the scenario (such as magnitude, distance and so on); $\mu_{base}(\vec{\xi})$ is the the median prediction of he ergodic base model; and $\vec{x}_e$ and $\vec{x}_s$ are the event and site coordinates, respectively. See e.g. Abrahamson et al. (2019); Villani and Abrahamson (2015); Walling and Abrahamson (2012) for more detailed descriptions.

In the following, we describe the (non-ergodic) GMM as a (Bayesian) hierarchical model. A observation (i.e., a recorded ground-motion parameter such as PGA or the response spectrum at a given period, denoted as Y_{es}, where e and s are indices for event and station) is distributed according to a normal distribution with median μ_{es} and standard deviation ϕ_0

$$Y_{es} \sim \mathcal{N}(\mu_{es}, \phi_0) \tag{2}$$

The median μ_{es} can be written as

$$\mu_{es} \sim \mu_{ERG_{es}} + f_{nonerg}(\vec{\theta}_{nonerg}; \vec{\xi}_{es}, \vec{x}_e, \vec{x}_s) + \delta B_e \tag{3}$$

where $\mu_{ERG_{es}}$ is the median prediction of the ergodic base model, and δB_e is the event term associated with event e. The term $f_{nonerg}(\vec{\theta}_{nonerg}; \vec{\xi}_{es}, \vec{x}_e, \vec{x}_s)$ describes the non-ergodic adjustment terms and subsumes the non-ergodic source, site, and path terms described in Equation (1). The event terms are distributed according to a normal distribution with mean zero and standard

deviation τ_0

$$\delta B \sim \mathcal{N}(0, \tau_0) \tag{4}$$

which can also be understood as the prior distribution for the event terms.

The median for the ergodic base model, $\mu_{ERG_{es}}$, consists of a GMM which is adjusted at small magnitudes ad distances to PIE events, and adjustment terms which account for regional differences between California and Oklahoma. It is described in Section Ergodic Base Model.

The individual non-ergodic adjustment terms are described subsequently in Section non-ergodic Adjustment Term. For model fitting purposes, the parameters of the adjustment model, $\vec{\theta}_{adj}$, which is part of $\mu_{ERG_{es}}$, are treated as fixed effects, while the systematic source, site and path effects (including the event terms δB) are treated as random effects. The parameters that control the distribution of the random effects (i.e. their standard deviations and/or correlation length scales) are referred to as hyperparameters in a Bayesian model.

5.1 Ergodic Base Model

The ergodic base model is developed from the model of Abrahamson et al. (2021) adjusted to Oklahoma conditions, and is written as

$$\mu_{ERGes} \sim f_{ASK21}(\vec{\xi})_{es} + f_{adj}(\vec{\theta}_{adj}; \vec{\xi}_{es}) \tag{5}$$

where $f_{ASK21}(\vec{\xi}_{es})$ is the median prediction of the ASK21 model, and $f_{adj}(\vec{\theta}_{adj}; \vec{\xi}_{es})$ is the adjustment due to differences between California and Oklahoma with $\vec{\theta}_{adj}$ parameters to be estimated; The different parts of the ergodic model are briefly described in Sections ASK21 Base Model and Regional Oklahoma Adjustment Term.

The model of Abrahamson et al. (2021), hereafter called ASK21, is itself an adjustment of the NGA W2 model of (Abrahamson et al., 2014) (ASK14) to induced data. The ASK21 model adjusts the ASK14 model to accommodate small magnitudes and short distances. However,

ASK21 retains the anelastic attenuation and linear site scaling coefficients of ASK14, meaning that it is valid for California conditions. In order to use ASK21 model, we include adjustment terms that account for differences in the anelastic attenuation and linear site scaling between California and Oklahoma. In addition to these adjustment terms, we also include an adjustment term for the strong moho bounce effect (Goulet et al., 2018, 2021) in the the Eastern and Central US, where Oklahoma resides, and which is not included in ASK14 nor ASK21. These regional adjustment terms are considered separate from the non-ergodic adjustment terms in the partially non-ergodic GMM development

5.1.1 ASK21 Base Model

Abrahamson et al. (2021) presents adjustments to Next Generation Attenuation West-2 (NGA-W2) GMMs for application to induced events. Abrahamson et al. (2021) noted that existing tectonic GMMs poorly model ground motion amplitudes from shallow rupture small magnitude events, generally underestimating short-period ground motion at distances less than 10 km for **M** less than 5. The ASK21 PIE GMM uses the ASK14 as the base model and adjusts magnitude dependence of the finite-fault term, $H(M)$, to accommodate magnitudes $M < 6$ with the term:

$$H(M) = \begin{cases} 4.5 & \text{for } M \geq 6 \\ \big(1.5 + 1.15(M - 5.57)\big) & \text{for } M < 6 \end{cases} \tag{6}$$

and adjusts the distance term at distances less than 15 km to accommodate small to moderate magnitudes at short-spectral periods with:

$$f_{adjust}(M, R_{rup}) = T_m(M) * \big(c_1 + f_R(R_{rup}, M)\big) \tag{7}$$

$$f_R(R_{rup}, M) = \begin{cases} c_2 * ln\Big(\frac{\max(R_{eff},5)+0.1}{R_c+0.1}\Big) & \text{for } R_{eff} < R_c \\ 0 & \text{for } R_{eff} \geq R_c \end{cases} \tag{8}$$

$$T_m(M) = \begin{cases} 1 & \text{for } M \leq 4 \\ \frac{5.5-M}{1.5} & \text{for } 4 < M < 5.5 \\ 0 & M \geq 5.5 \end{cases} \tag{9}$$

in which c_2 is a coefficient; R_{eff} is the effective rupture distance and $\max(R_{eff}, 5)$ term models distance dependence saturation at 5 km or less; R_c is the distance at which geometrical spreading term is adjusted in the ASK21 GMM.

5.1.2 Regional Oklahoma Adjustment Term

The regional adjustment term is to model the regional differences between California (the source region of ASK14 and ASK21) and Oklahoma. The adjustment term is as follows

$$f_{adj}(\vec{\theta}_{adj}; \vec{\xi}_{es}) = c_0 + c_1 lnR_{50} + c_2 \ln \frac{V_{S30}}{760} - f_{attn,ASK21}(R) + c_3 R \tag{10}$$

in which c_0 is the global regional adjustment term; $c_1 lnR_{50}$ accounts for the Moho bounce seen in the data, as shown by Figure 3; $c_2 \ln \frac{V_{S30}}{760}$ accounts for differences in the linear site scaling between California and Oklahoma that is attributed to differences in the average reference profile; c_3 is the regional distance adjustment term.

Figure 3 shows residuals to ASK21 of the full dataset, with records at one station (KAN15) highlighted. One can clearly see a positive trend from about 50km to 200km, which is modeled through $c_1 lnR_{50}$, where

$$lnR_{50} = \begin{cases} 0 & R < 50 \\ \ln \sqrt{R^2 + H(M)^2} - \ln \sqrt{50^2 + H(M)^2} & 50 \leq R \leq 200 \\ \ln \sqrt{200^2 + H(M)^2} - \ln \sqrt{50^2 + H(M)^2} & 200 < R \end{cases} \tag{11}$$

and $H(M)$ is defined as in Equation (6). Similar to Kuehn et al. (2019), we remove the intrinsic anelastic attenuation term $f_{attn,ASK21}(R)$ from the base ASK21 GMM so that it can be included as part of the adjustment here.

In setting up our regression analysis, c_0, c_1, c_2 and c_3 are fixed effects that required priors. Because we have a large data set, we adopted weakly informative prior distributions for these

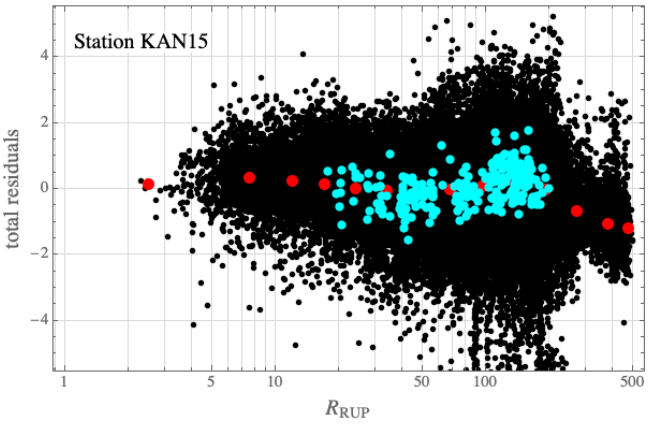

Figure 3: Total residuals to the ASK21 model wih anelasitc attenuation removed for all stations (black), mean residual in different distance bins (red), and residuals for station KAN15.

fixed effects as the data should be sufficient to estimate them well. These priors were

$$c_0 \sim N(0, 0.45) \tag{12}$$

$$c_1 \sim N(0, 10) \tag{13}$$

$$c_2 \sim N(0, 10) \tag{14}$$

$$c_3 \sim N(-0.01, 0.01) \tag{15}$$

Except for c_3, all are centered at 0. For c_3 the mean is set to -0.01 because it represents anelastic attenuation, which should be negative; however, when we performed the regression we did not constrain c_3 to be negative because we favored the normal distribution for the prior, and we noticed that at spectral periods greater than 0.5 seconds c_3 trended towards a positive value.

Although the data may be better fit with a positive linear R term, this behavior will not extrapolate properly to large distances. Because in PSHA, GMMs are often applied outside the range constrained by data, we don't allow for positive c_3 coefficients. We removed c_3 coefficient from our adjustment term $f_{adj}(\vec{\theta}_{adj}; \vec{\xi}_{es})$ term at spectral periods greater than 0.5 seconds to eliminate this undesired effect. The final $f_{adj}(\vec{\theta}_{adj}; \vec{\xi}_{es})$ function of the partially non-ergodic model was then:

$$f_{adj}(\vec{\theta}_{adj};\vec{\xi}_{es}) = \begin{cases} c_0 + c_1 lnR_{50} + c_2 \ln\frac{V_{S30}}{760} - f_{attn,ASK21}(R) + c_3 R & \text{for } T \leq 0.5 \\ c_0 + c_1 lnR_{50} + c_2 \ln\frac{V_{S30}}{760} - f_{attn,ASK21}(R) & \text{for } 0.5 < T \end{cases} \tag{16}$$

5.2 non-ergodic Adjustment Term

The non-ergodic adjustment term comprises a varying coefficient model (Gelfand et al., 2003; Landwehr et al., 2016) and a cell-specific anelastic attenuation model (Dawood and Rodriguez-Marek, 2013; Kuehn et al., 2019). The non-ergodic adjustment has the form

$$f_{nonerg}(\vec{\theta}_{nonerg};\vec{\xi}_{es},\vec{x}_e,\vec{x}_s) = f_{eq}(\vec{x}_e) + \overrightarrow{\Delta R}(\vec{x}_s,\vec{x}_s)\cdot\vec{c}_{ca} + \delta S2S_s \tag{17}$$

where $f_{eq}(\vec{x}_s)$ is a spatially varying systematic source term, $\overrightarrow{\Delta R}\cdot\vec{c}_{ca}$ describes the cell-specific attenuation term. The cell-specific attenuation term is the dot product of $\overrightarrow{\Delta R}$, a vector of path lengths within each cell, and the vector of cell-specific attenuation coefficients $\vec{c}_{ca}$. $\delta S2S$ is a (non-spatially varying) systematic site term.

Contrary to other non-ergodic models (Caramenti et al., 2020; Kuehn, 2021c; Landwehr et al., 2016; Lanzano et al., 2021; Lavrentiadis et al., 2021; Sung et al., 2021) we do not include a spatially correlated site term. The average distance between stations in our dataset is large, which does not allow one to reliably infer the spatial length scale of spatially correlated site terms. Only the spatially independent site terms, $\delta S2S_s$, are included in the model.

Following Landwehr et al. (2016), we model the spatially varying source term $f_{eq}(\vec{x}_e)$ as a Gaussian random field/Gaussian process. This encodes a notion that nearby events produce similar event terms (Kuehn and Abrahamson, 2020; Trugman and Shearer, 2018). The $f_{eq}(\vec{x}_e)$ field is parameterized by a mean function, which is zero in this case because the term is an adjustment to an ergodic base model, and a covariance function, which determines how strongly correlated nearby events are with one another.

For the covariance function of $f_{eq}(\vec{x}_e)$, we use the Matérn covariance function, which is

widely used in spatial statistics:

$$k(\vec{x}, \vec{x}') = \omega^2 \frac{2^{(1-\nu)}}{\Gamma(\nu)} (\kappa|\vec{x} - \vec{x}'|)^\nu K_\nu(\kappa|\vec{x} - \vec{x}'|) \tag{18}$$

where Γ is the Gamma function, K_ν is the modified Bessel function of the second kind, κ is a scale parameter and ν is a smoothness parameter. For $\nu = 0.5$, the Matérn covariance function becomes the exponential covariance function, while for $\nu \to \infty$ it becomes the squared exponential covariance function (Rasmussen and Williams, 2006). Generally, the larger the ν, the smoother the process. We use a value $\nu = 1$, which is the default in INLA for two-dimensional data (Bakka et al., 2018; Lindgren and Rue, 2015). Kuehn (2021c) showed that results from INLA, using a Matérn covariance with $\nu = 1$, are very similar to results obtained using a exponential covariance function, which is used in other non-ergodic GMMs based on VCMs (Landwehr et al., 2016; Lavrentiadis et al., 2021; Sung et al., 2021). The spatial field then serves as the prior distribution for the systematic event terms:

$$f_{eq} \sim GF(0, k(\vec{x}, \vec{x}'))$$

where the covariance function $k(\vec{x}, \vec{x}')$ is the Matérn function of Equation (18).

For the for the hyperparameters of f_{eq}, we use a penalized complexity (PC) prior (Franco-Villoria et al., 2019; Simpson et al., 2017). In the PC framework, the spatial model is seen as a complex extension to a simpler, non-spatial base model, encoding shrinkage towards the base model. The PC prior favors the simpler model and does only allow the more complex model if the data strongly favors it. The hyperparameters associated with the spatial field are the marginal standard deviation ω and the range $\ell = \frac{\sqrt{8\nu}}{\kappa}$ (Krainski et al., 2019), which corresponds to the distance where the correlation has a value of 0.14. The PC prior for a two-dimensional spatial field with Matérn covariance function was developed by Fuglstad et al. (2019) and is specified by setting probabilities for the marginal standard deviation and the range. We use

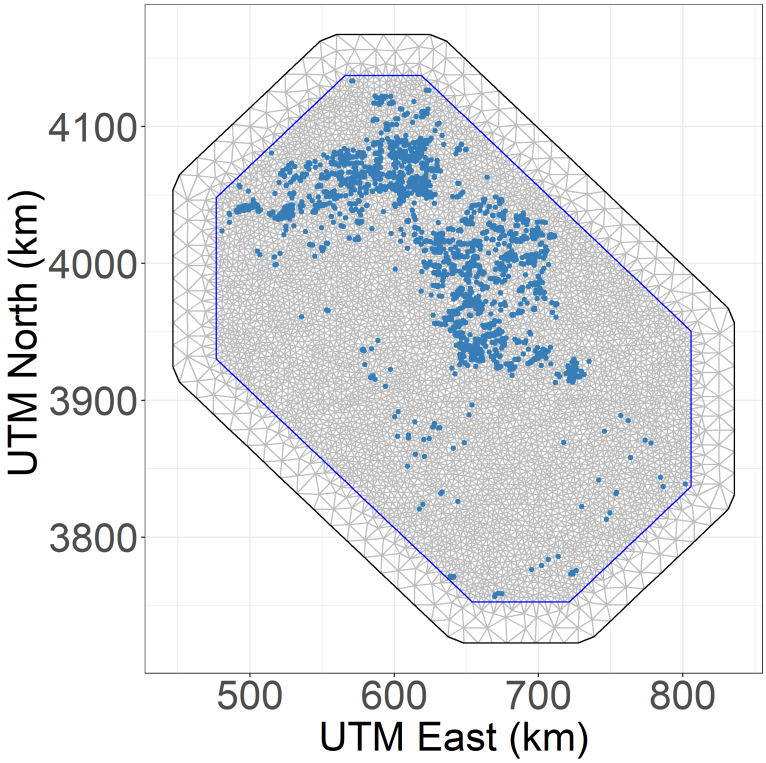

Figure 4: Mesh used for modeling the systematic source effects.

the following values to specify the PC prior

$$Pr(\omega > 0.23) = 0.01 \tag{19}$$

$$Pr(\ell < 10.0) = 0.5 \tag{20}$$

Using the discussed parameterization of f_{eq} mean and hyperparameters, the spatially varying systematic source terms of $f_{eq}(\vec{x}_e)$ are encoded at the nodes of the input mesh following the SPDE approach in INLA. We used the input mesh shown in Figure 4 for $f_{eq}(\vec{x}_e)$, which was created from the source locations.

The cell-specific attenuation are modeled similar to Kuehn et al. (2019). To implement this into our model, the study region was divided into at 0.15 degree by 0.15 degree cells, the number of paths in each cell were computed, and the cell-adjustment terms were given a normal prior distribution as in Kuehn et al. (2019):

$$c_{ca} \sim N(0, \omega_{ca})$$

The prior distribution for ω_{ca} is also based on the PC-prior. In this case, we specify a probability α and a value u such that $Pr(\omega_{ca} > u) = \alpha$. For the cell-specific attenuation, the values were informed by (Kuehn et al., 2019), and we use the following prior:

$$Pr(\omega_{ca} > 0.01) = 0.01 \tag{21}$$

Lastly, prior distribution for the non-spatially varying station term is the normal distribution:

$$\delta S2S \sim N(0, \phi_{S2S})$$

When developing the cell-specific attenuation coefficients $\vec{c}_{ca}$ component of the model, we were interested in the coupled behavior of $\vec{c}_{ca}$ with the anelastic attenuation coefficient c_3, which we desired to be negative when combined. At spectral periods near 0.3, around 10 percent of the combination trended towards positive values, which increased with increasing period. We felt that 10 percent was a good threshold to determine that the cell-specific attenuation $\vec{c}_{ca}$ should be removed from the model. Subsequently, at spectral periods greater than 0.3 seconds $\vec{c}_{ca}$ was removed and the final functional form adopted for the non-ergodic adjustment was then

$$f_{nonerg}(\vec{\theta}_{nonerg}; \vec{\xi}_{es}, \vec{x}_e, \vec{x}_s) = \begin{cases} f_{eq}(\vec{x}_e) + \overrightarrow{\Delta R}(\vec{x}_s, \vec{x}_s) \cdot \vec{c}_{ca} + \delta S2S_s & \text{for } T \leq 0.3 \\ f_{eq}(\vec{x}_e) + \delta S2S_s & \text{for } 0.3 < T \end{cases} \tag{22}$$

5.3 Prior Distributions for Standard Deviation Hyperparameters

The standard deviations ϕ_0, τ_0, $\phi_{S2S,0}$ are internally represented as precision, which is the inverse of the variance (i.e. $prec_\tau = \frac{1}{\tau^2}$). When estimating the coefficients, we placed a Gamma prior on the precision parameters (more precisely, a log-Gamma prior on the logarithmic precision),

with shape parameter 2 and rate parameter 0.5:

$$\ln prec_{\tau} \sim \ln G(2, 0.5) \tag{23}$$

$$\ln prec_{\phi_0} \sim \ln G(2, 0.5) \tag{24}$$

$$\ln prec_{\phi_{S2S,0}} \sim \ln G(2, 0.5) \tag{25}$$

This implies a prior mean for a precision of $4. = 2/0.5$.

6 Results

The final partially non-ergodic PIE model coefficients were computed at spectral periods where there were sufficient data in the final dataset to estimate the coefficients. These were spectral periods 0.01, 0.1, 0.15, 0.2, 0.25, 0.3, 0.4, 0.5, 0.75, 1.0, and 1.5 seconds. All model coefficients were estimated using Eq. 2. The final functional form adopted for the induced partially non-ergodic mean ground-motion model is shown in Equation (26).

$$\mu_{es} = f_{ASK21}(\vec{\xi})_{es} + c_0 + c_1 ln R_{50} + c_2 \ln \frac{V_{S30}}{760} - f_{attn,ASK21}(R) + \delta S2S_s + \delta B_e + f_{eq}(\vec{x}_e) + \Delta$$

$$\Delta = \begin{cases} \overrightarrow{\Delta R}(\vec{x}_s, \vec{x}_s) \cdot \vec{c}_{ca} + c_3 R & \text{for } T \leq 0.3 \\ c_3 R & \text{for } 0.3 < T \leq 0.5 \\ 0 & \text{for } T > 0.5 \end{cases} \tag{26}$$

Figures 5, 6, 7, and 8 show the final adjustment coefficients for c_0, c_1, c_2 and c_3 derived respectively, with error bars showing the 5^{th} and 95^{th} uncertainty range. Using Equation (26) as a reference for the partially non-ergodic GMM, NERG-M1 references when $\Delta = \overrightarrow{\Delta R}(\vec{x}_s, \vec{x}_s) \cdot \vec{c}_{ca} + c_3 R$; NERG-M2 references when $\Delta = c_3 R$; and NERG-M3 references when $\Delta = 0$. Figure 9 shows the systematic spatial non-ergodic $f_{eq}(\vec{x}_e)$ PGA mean terms and Figure 10 shows the standard deviation. These figures show that for PGA higher-ground motions are predicted in the north and south-east region of the study area from source effects and in the area where the

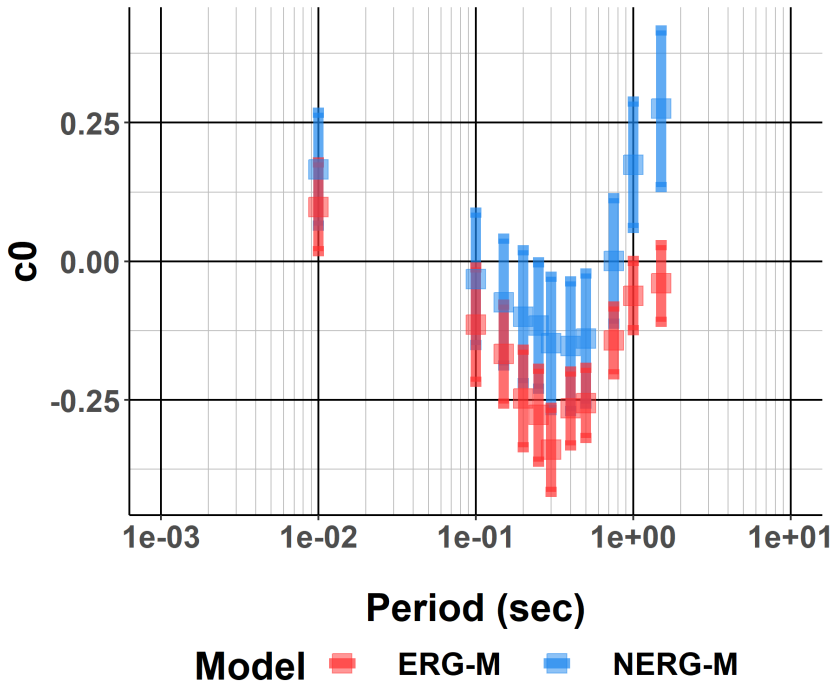

Figure 5: c0 - intercept

earthquake locations are concentrated the variability of $f_{eq}(\vec{x}_e)$ is small. The other non-ergodic component of the model, the cell-specific attenuation is shown in Figure 12 for the PGA mean values and Figure 13 for the standard deviation. The number of paths in each cell is shown in Figure 14.

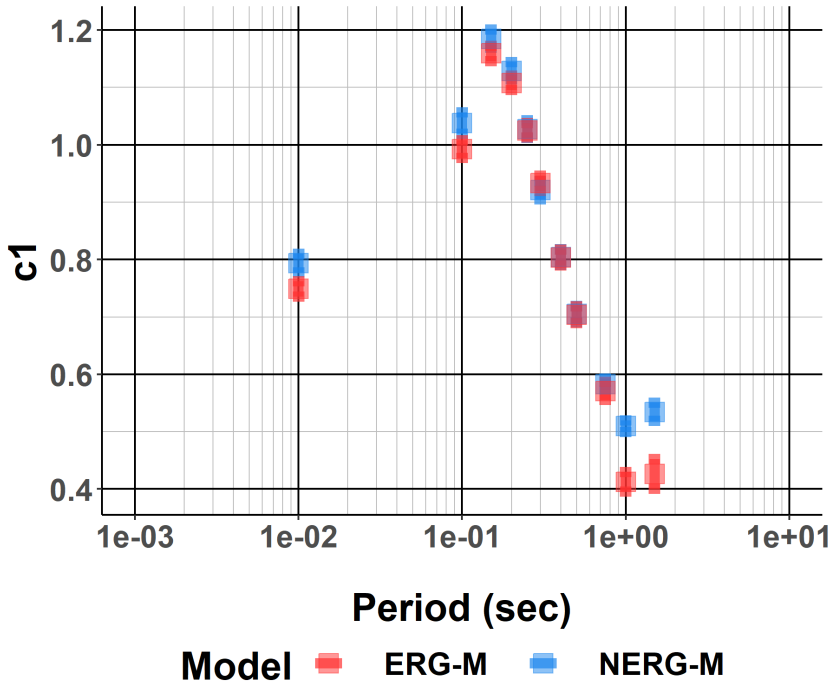

Figure 6: c1 - moho bounce

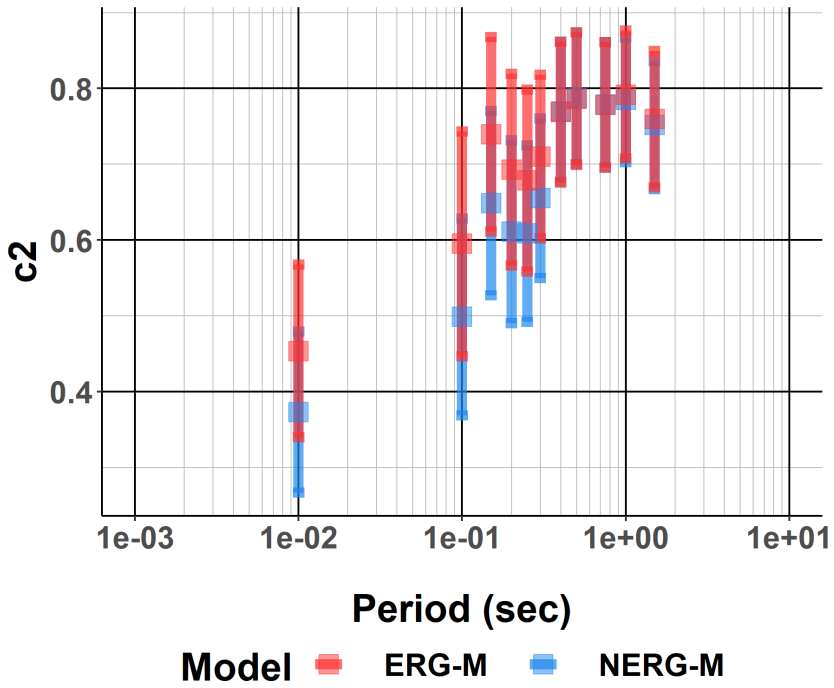

Figure 7: c2 - site

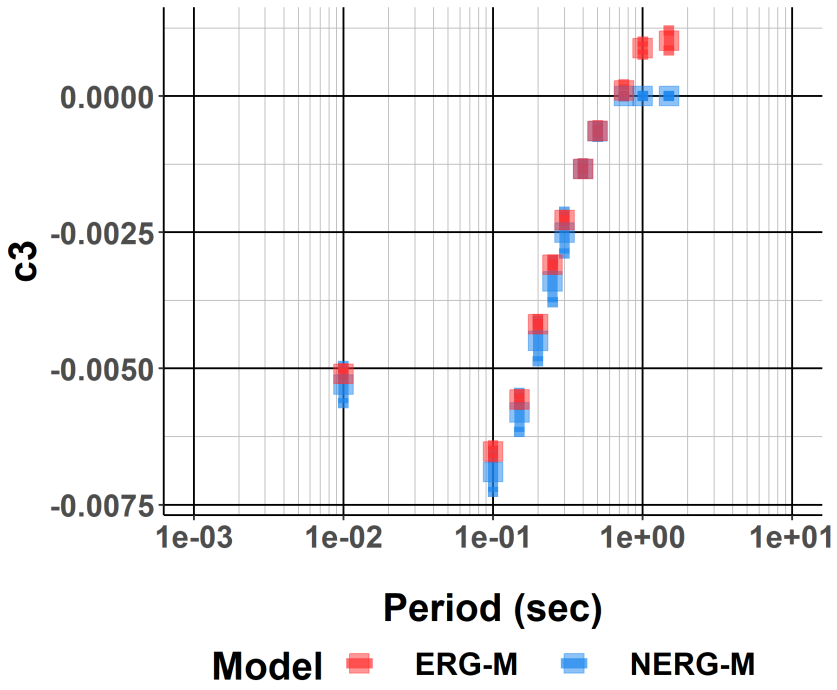

Figure 8: c3 - distance

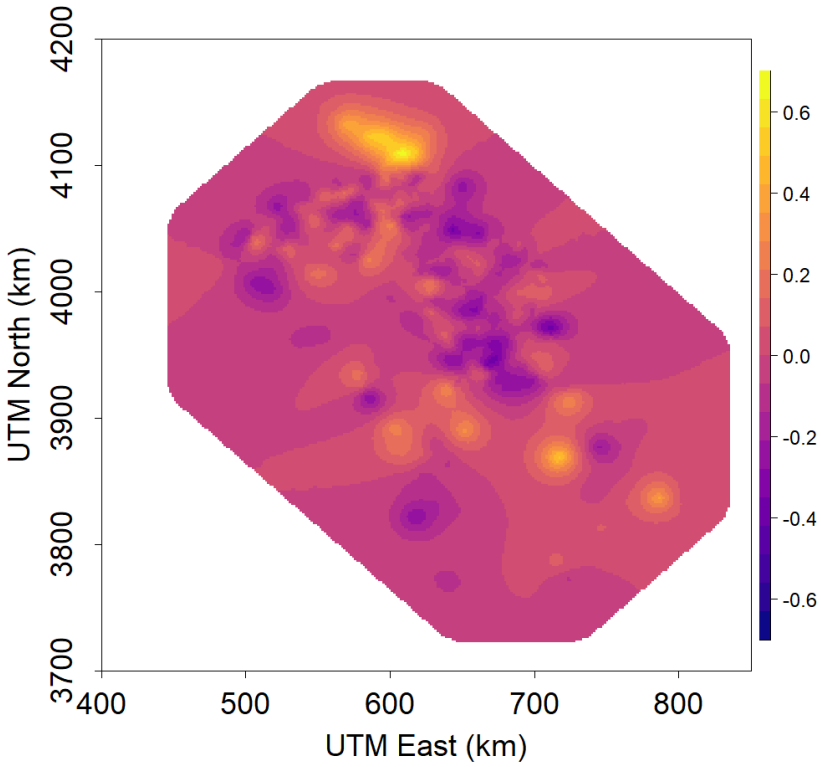

Figure 9: Mean

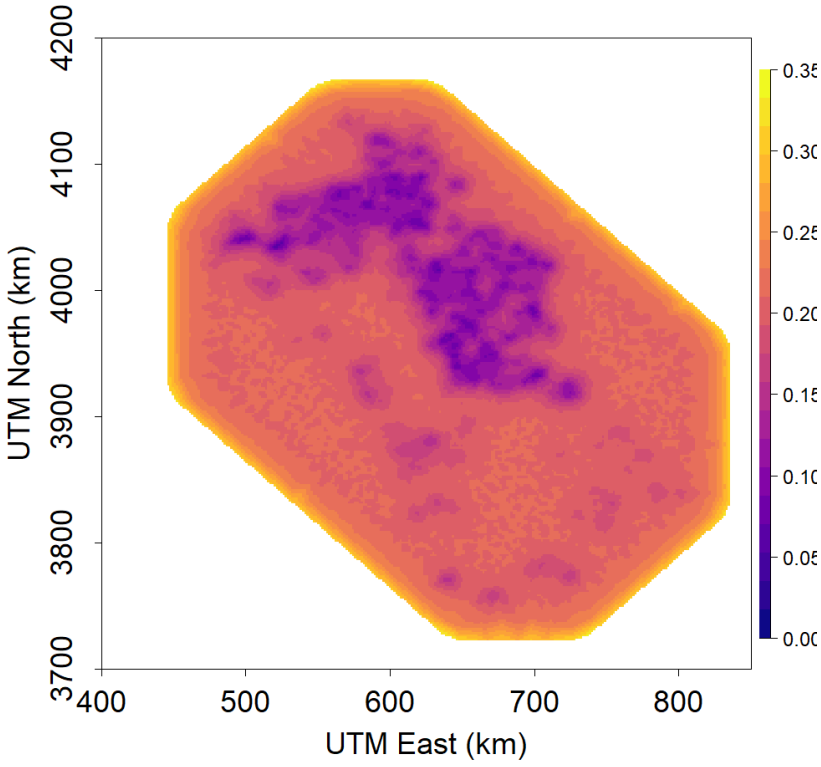

Figure 10: Std Dev

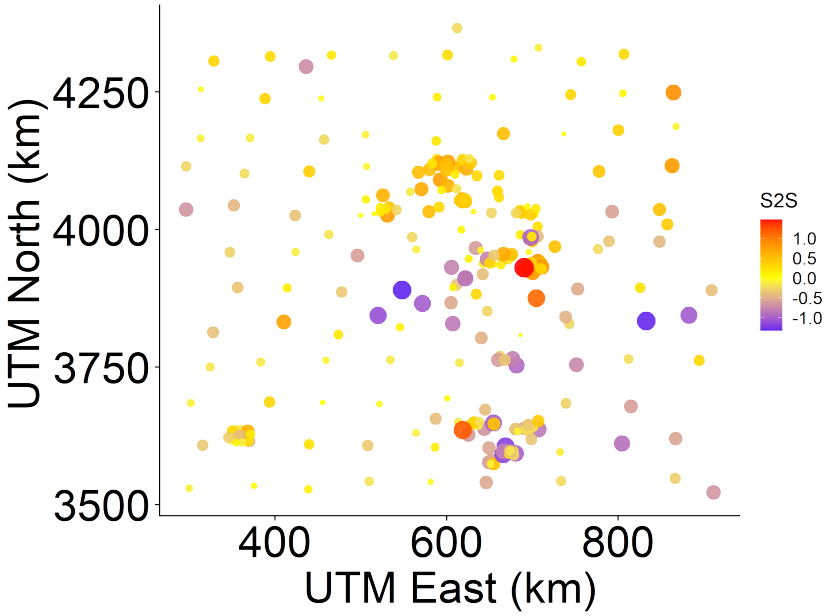

Figure 11: PGA station terms map

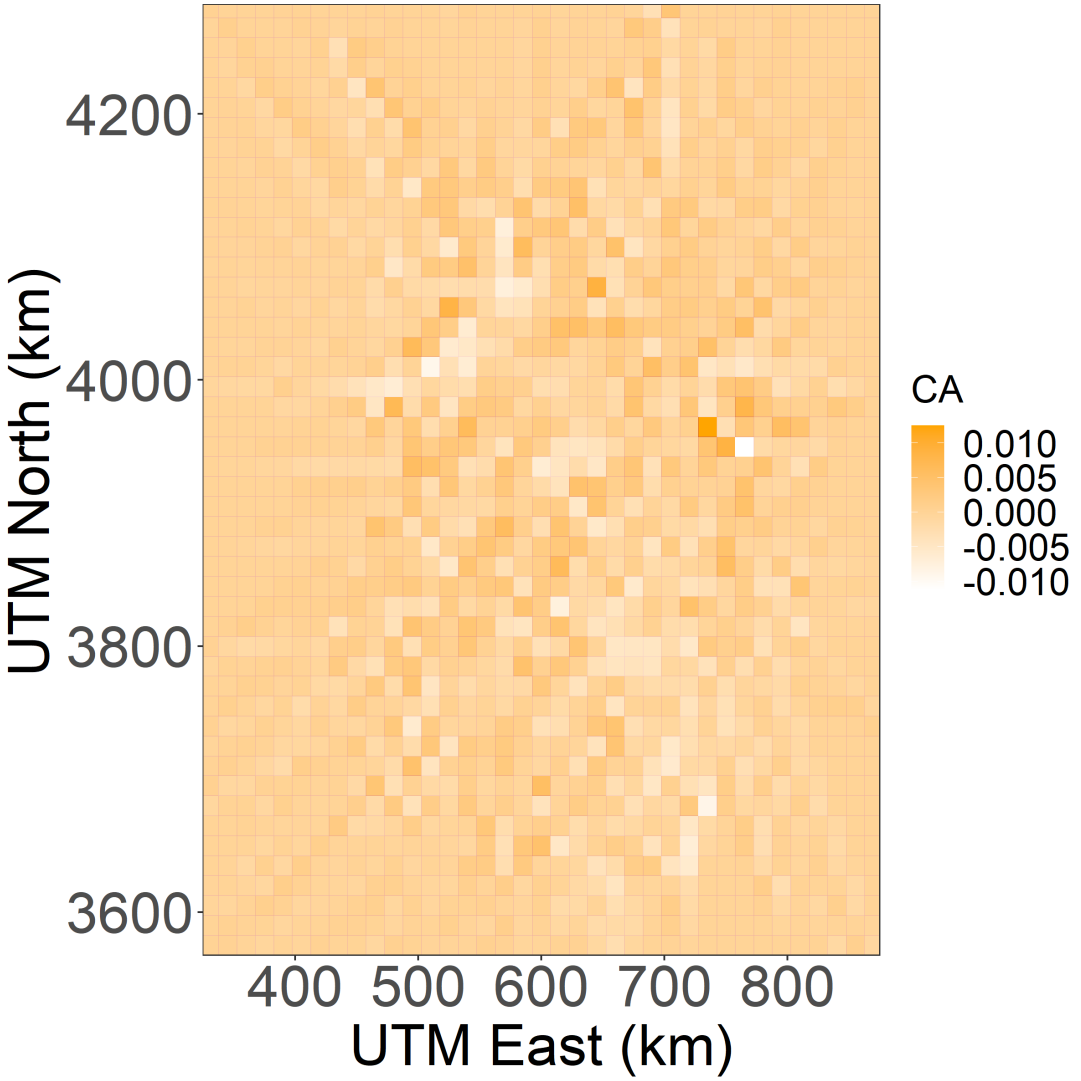

Figure 12: cA mean

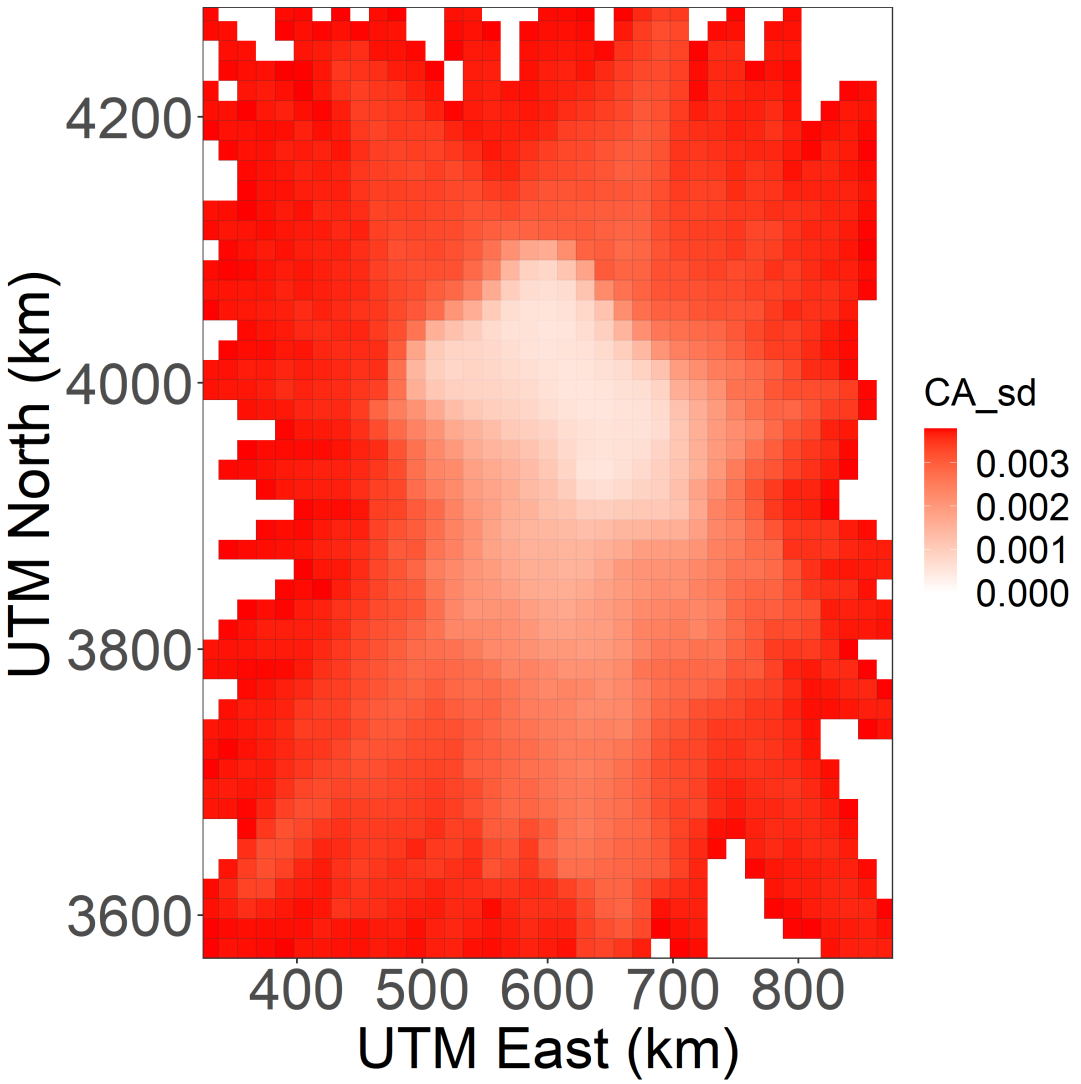

Figure 13: cA sd

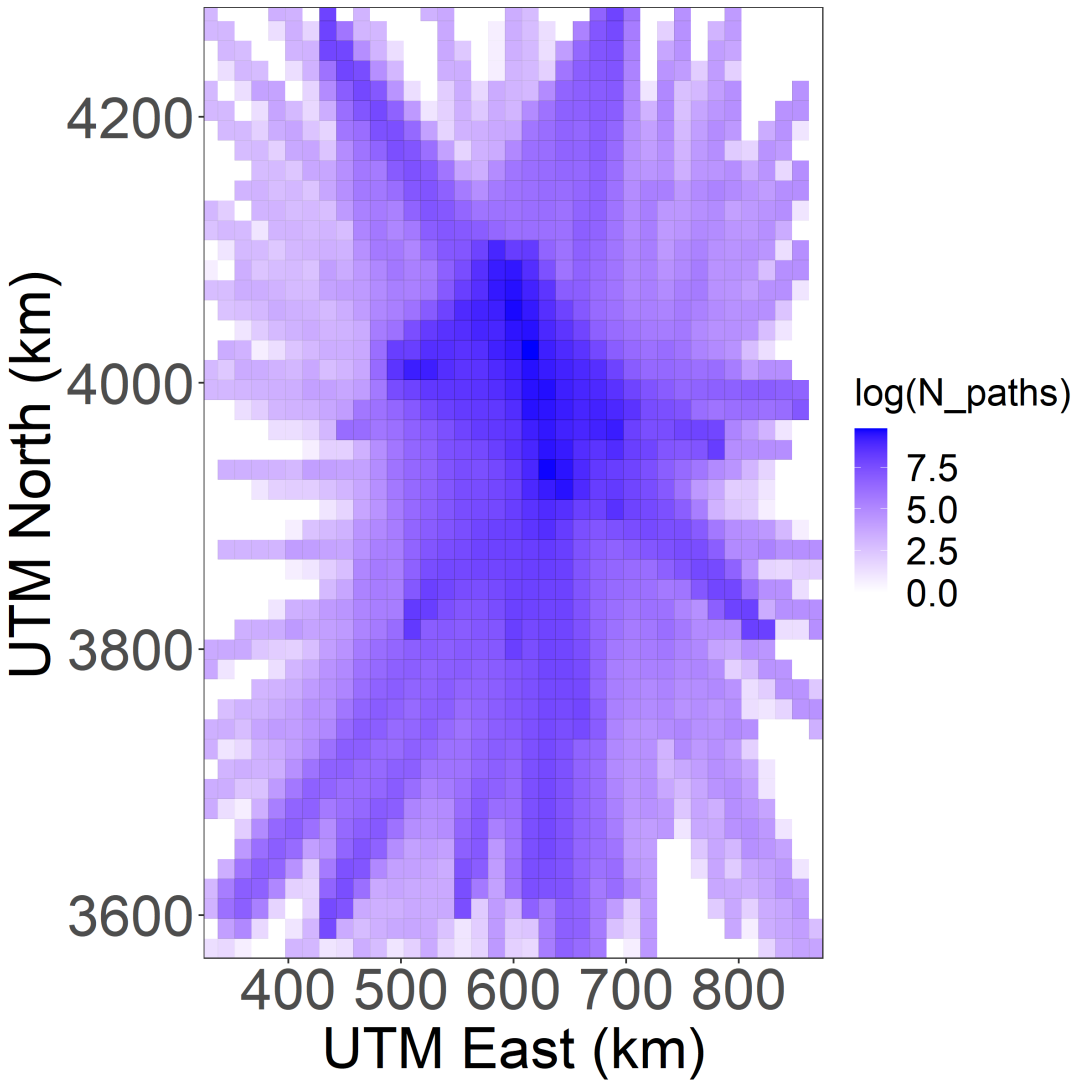

Figure 14: Number of paths

The ϕ_{S2S}, ϕ_{SS} and τ_{eq} hyperparameters versus spectral period are presented in Figures 15, 16, and 17, respectively. These figures show that PNREG-M1 hyperparameters are between 10 to 20 percent lower than ERG-M hyperparameters. Once the non-ergodic cell-specific attenuation c_{ca} are removed PNREG-M1,M2 coefficients are similar to ERG-M coefficients for site hyperparameters ϕ_{S2S} anf ϕ_{SS}. In contrast, the PNREG-M1,M2,M3 τ_{eq} coefficients are consistently lower than ERG-M coefficients across all periods. This is likely a result of including spatially varying systematic event terms, $f_{eq}(\vec{x}_e)$, in the partially non-ergodic models.

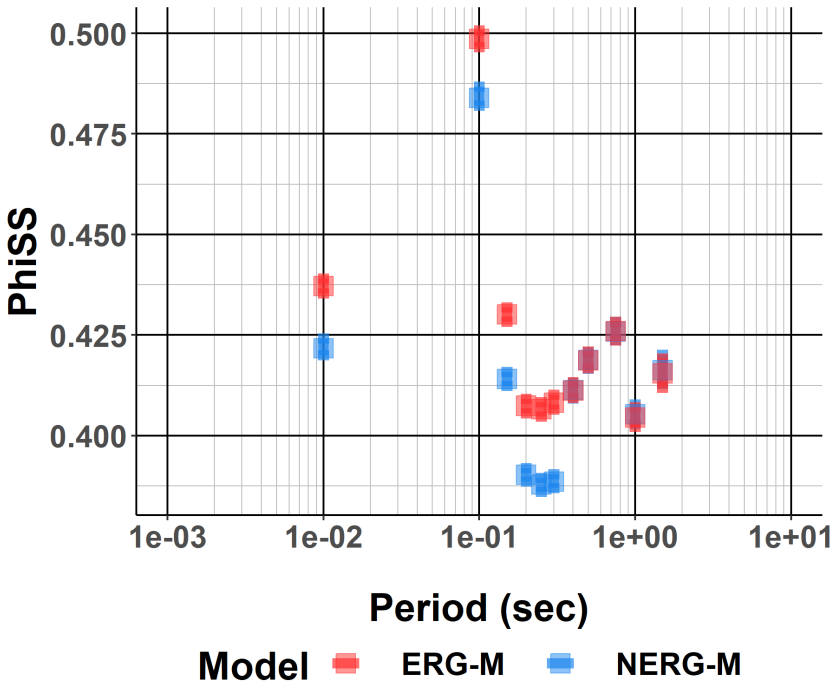

Figure 15

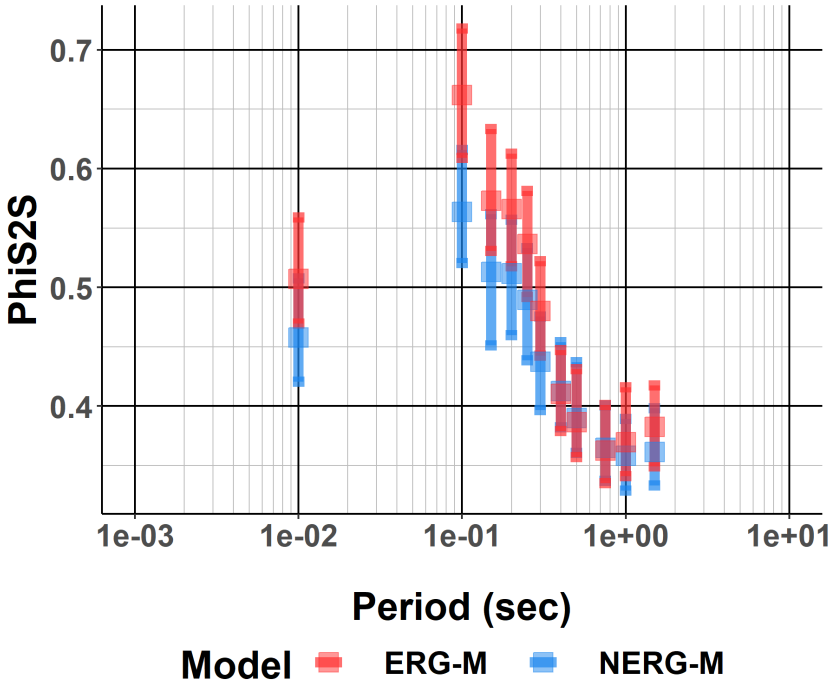

Figure 16

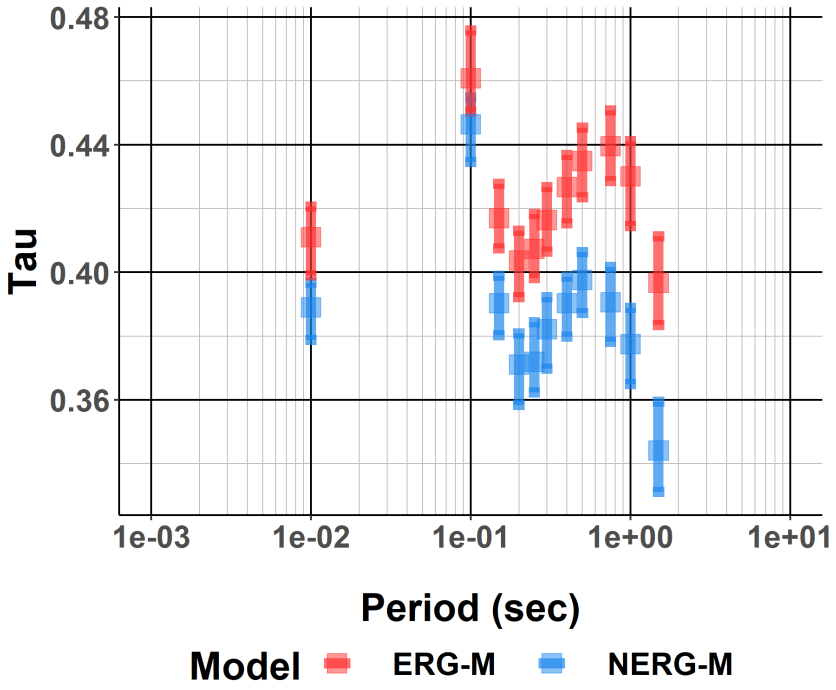

Figure 17

7 Model Applicability

The final partially non-ergodic model is applicable to PIE events occurring within the Oklahoma region at distances less than 300 km from the site and for spectral periods less than or equal to 1.5 secs.

8 Response Spectra

Response spectra plots of Mw 5.5 at hypocentral distances of 20 km, 50 km, 100 km and 200 km are shown in Figures 18, 19,20, and 21, respectively, and compared to the ASK2021 GMM. The NREG-M and the ERG-M show lower ground motions at distances less than 100 km, and larger ground motions at distances greater than 100 km. The ASK21 GMM is developed using California data, and the differences in the attenuation from the west and east are picked up in the NREG-M. Recall that the magnitude conversion has a large effect on the residuals for the Oklahoma ground motions. In this study, the magnitudes for small magnitude events that were converted to moment magnitude (set 2) were used as reported. In contrast, the ASK21 GMM

applied a correction to the set 2 magnitudes. If the non-ergodic GMM was developed using the same conversion as used in the ASK21 GMM, the ERG-M and NERG-M models would have larger ground motions, closer to the ASK21 GMM at short distances. The differences in the large distance scaling would be similar to those shown here.

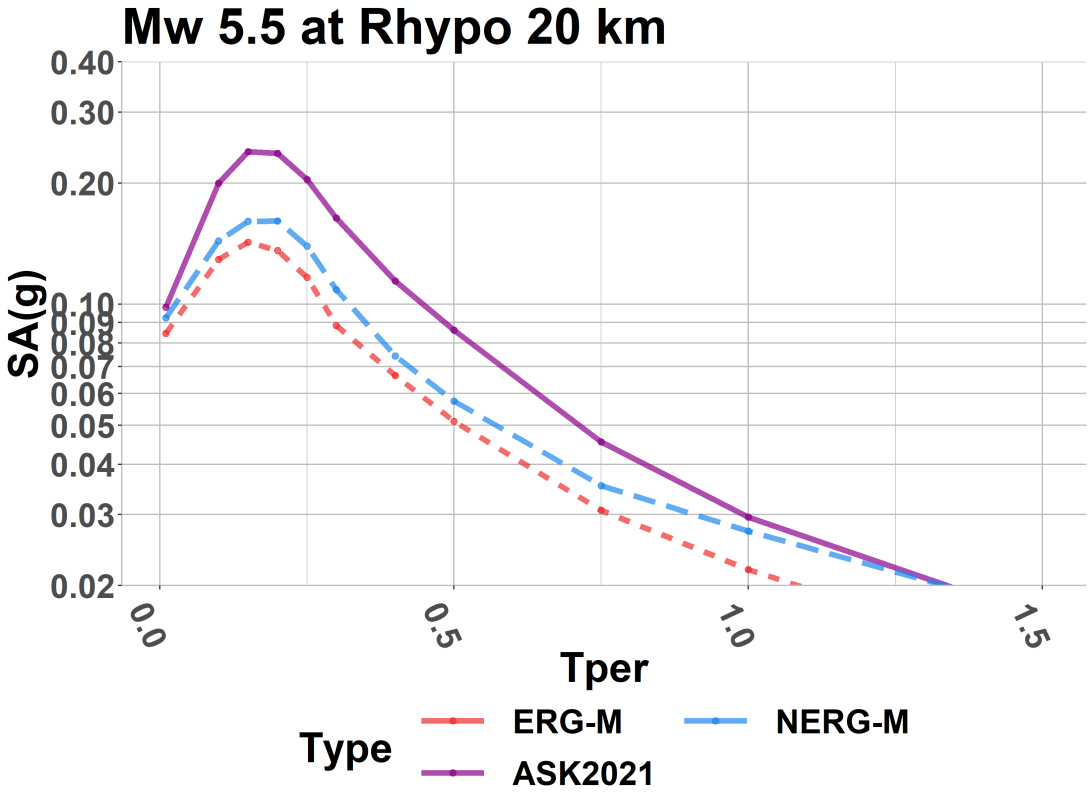

Figure 18: Rhypo 20 km

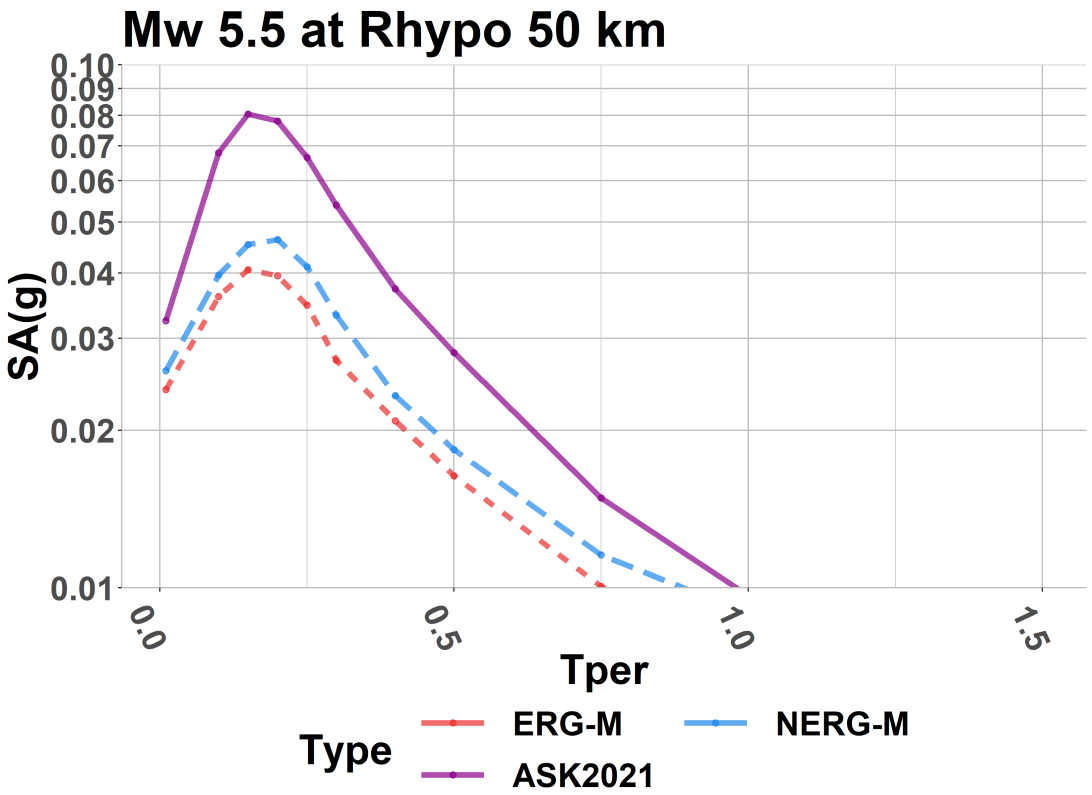

Figure 19: Rhypo 50 km

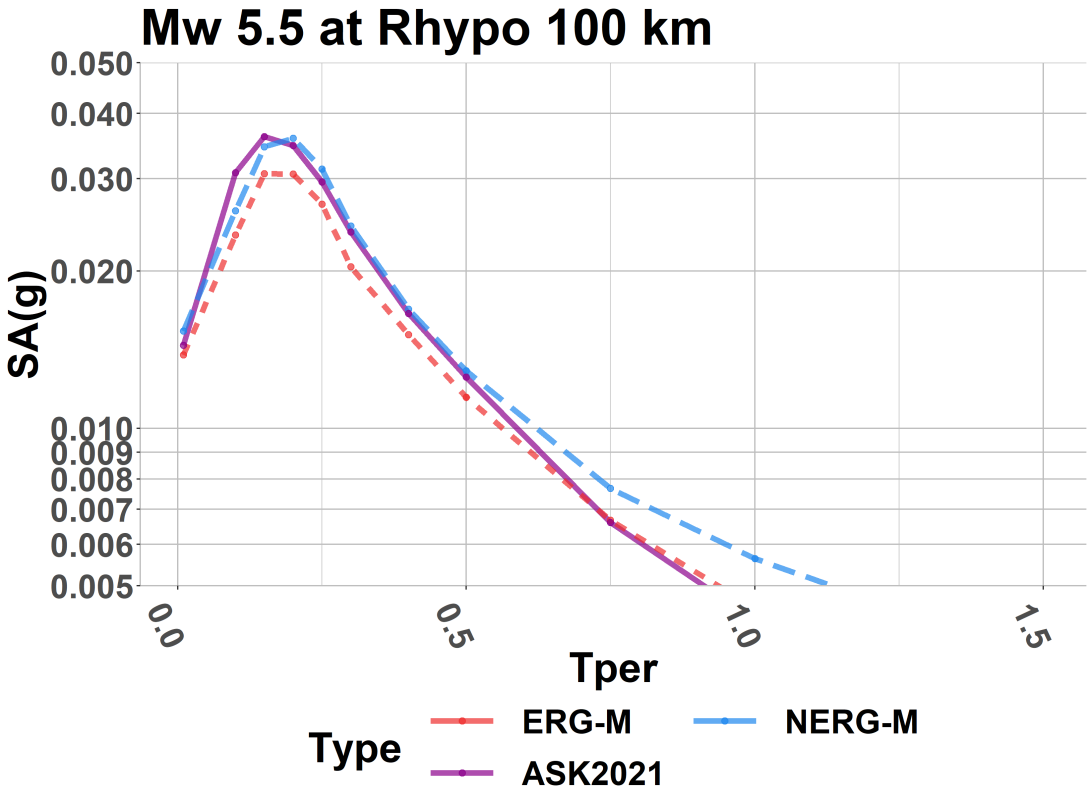

Figure 20: Rhypo 100 km

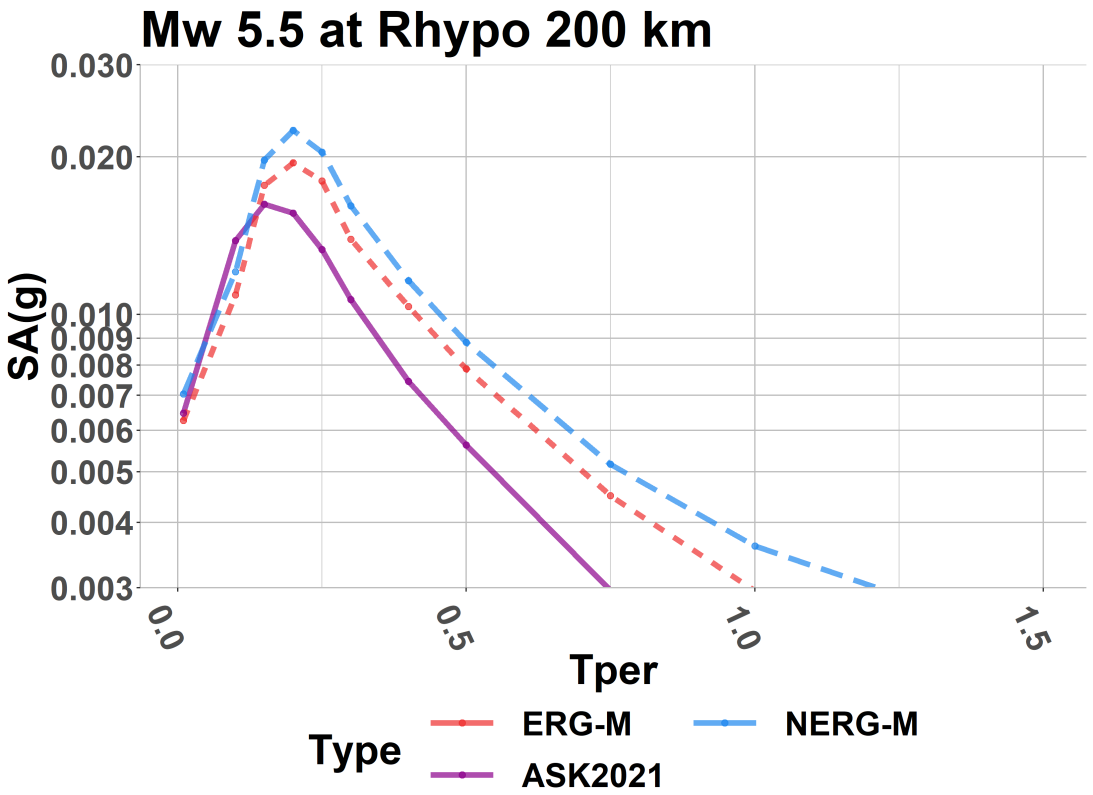

Figure 21: Rhypo 200 km

9 Magnitude and Distance Scaling Effects

Magnitude scaling of the NREG-M is shown in Figure 22 at hypocentral distance of 20 km and Figure 23 at hypocentral distance of 75 km at spectral periods 0.01 (PGA), 0.2 second and 1 second. The solid line represents the ASK21 GMM scaling, the long-dashed line represents the NERG-M scaling and the small dashed line represents the ERG-M scaling. These figures show little differences in magnitude scaling between the three models.

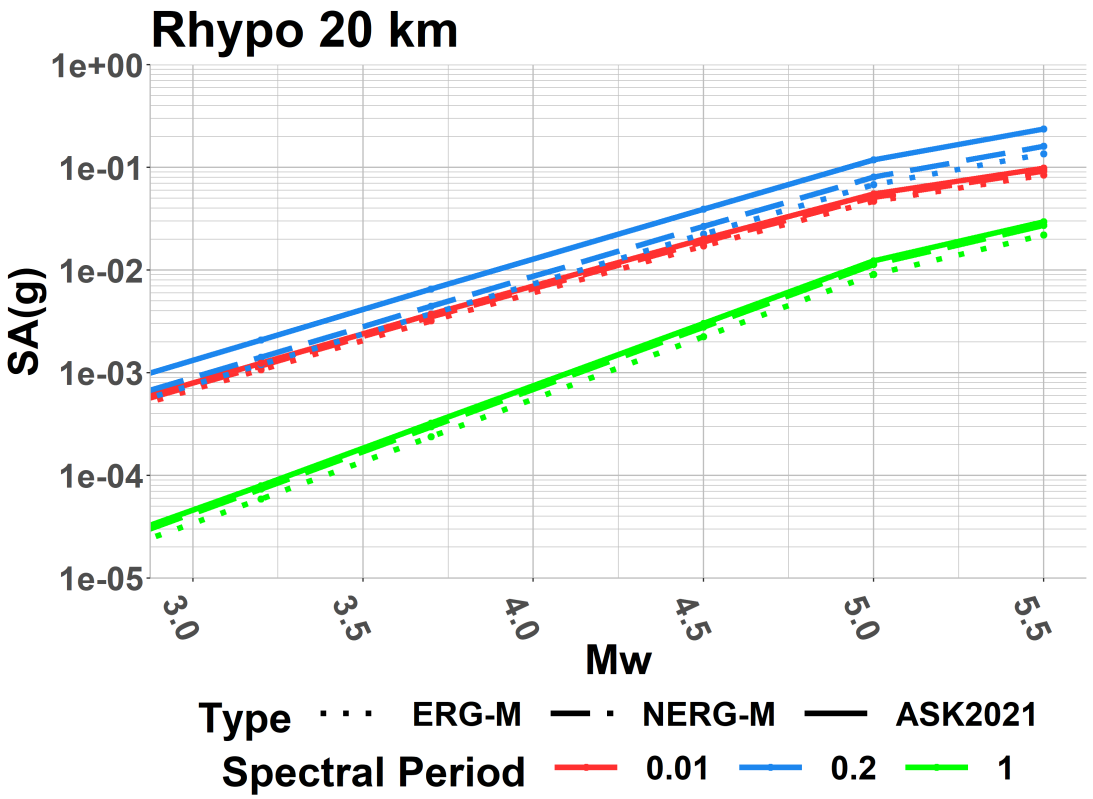

Figure 22: Rhypo 20 km

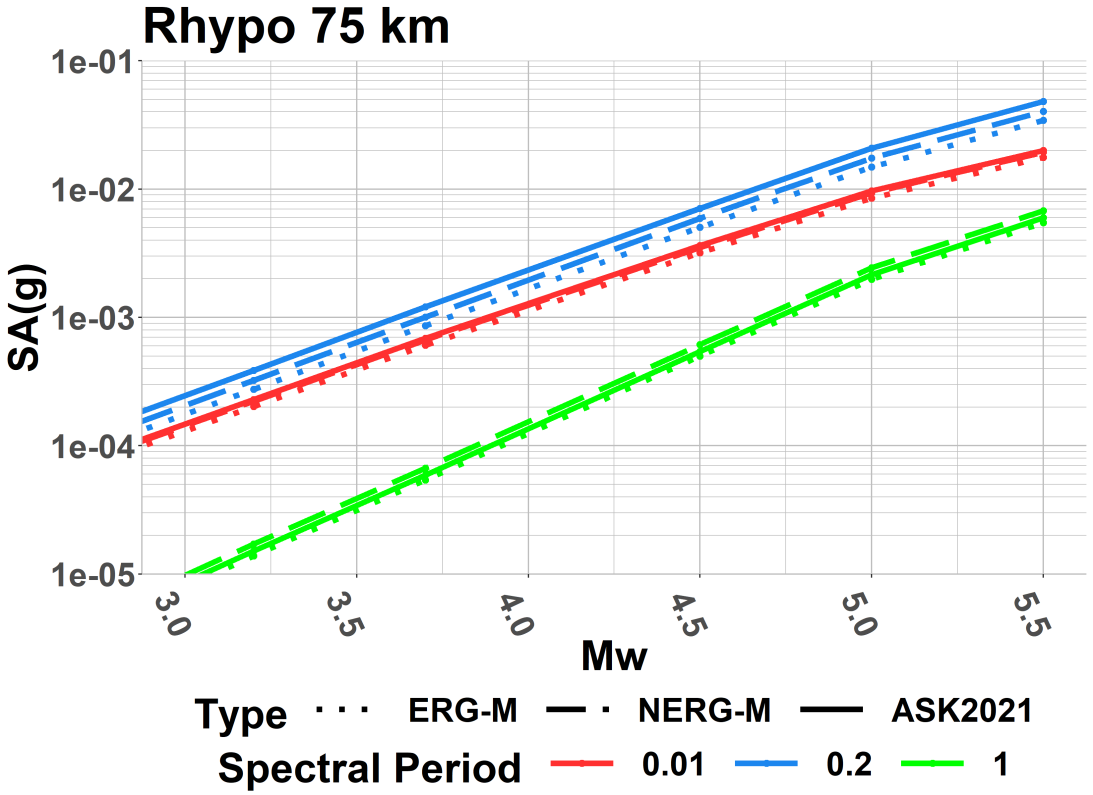

Figure 23: Rhypo 75 km

Distance scaling of the PNREG-M is compared to the ERG-M and ASK2021 in Figure 24

. This figure shows that models generally share a similar distance scaling

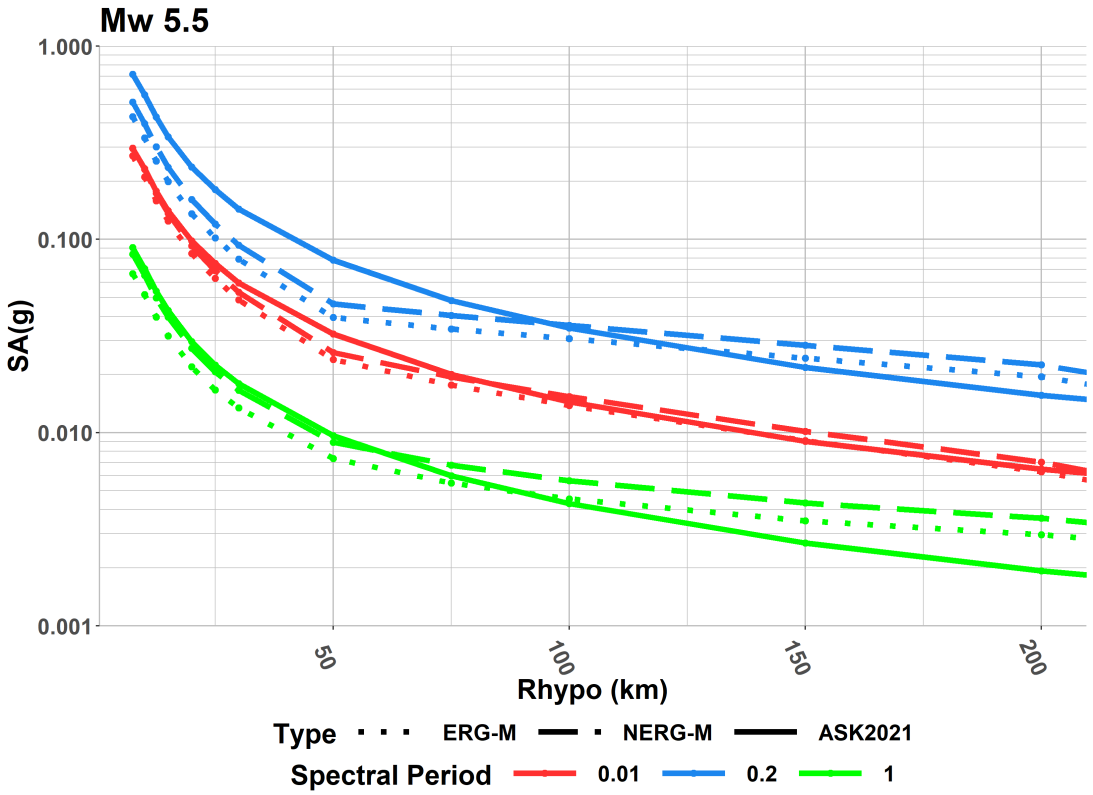

Figure 24: Mw 5.5

Site scaling with V_{S30} of the NERG-M is compared to the ERG-M and ASK2021 in Figure 25 for Mw 5. This figure shows a larger divergence between the ASK21 GMM and the NERG-M and ERG-M models in the site-scaling. The NERG-M and ERG-M site scaling appears to be relatively constant with V_{S30}. For an oscillator period of 1.0 seconds, the scaling of spectral acceleration with V_{S30} is positive. Such a scaling is physically implausible. For use of our GMM, the total V_{S30}-scaling coefficient should be constrained to be negative (i.e. the value of coefficient c_2 should be smaller than the absolute value of the ASK21 V_{S30} coefficient).

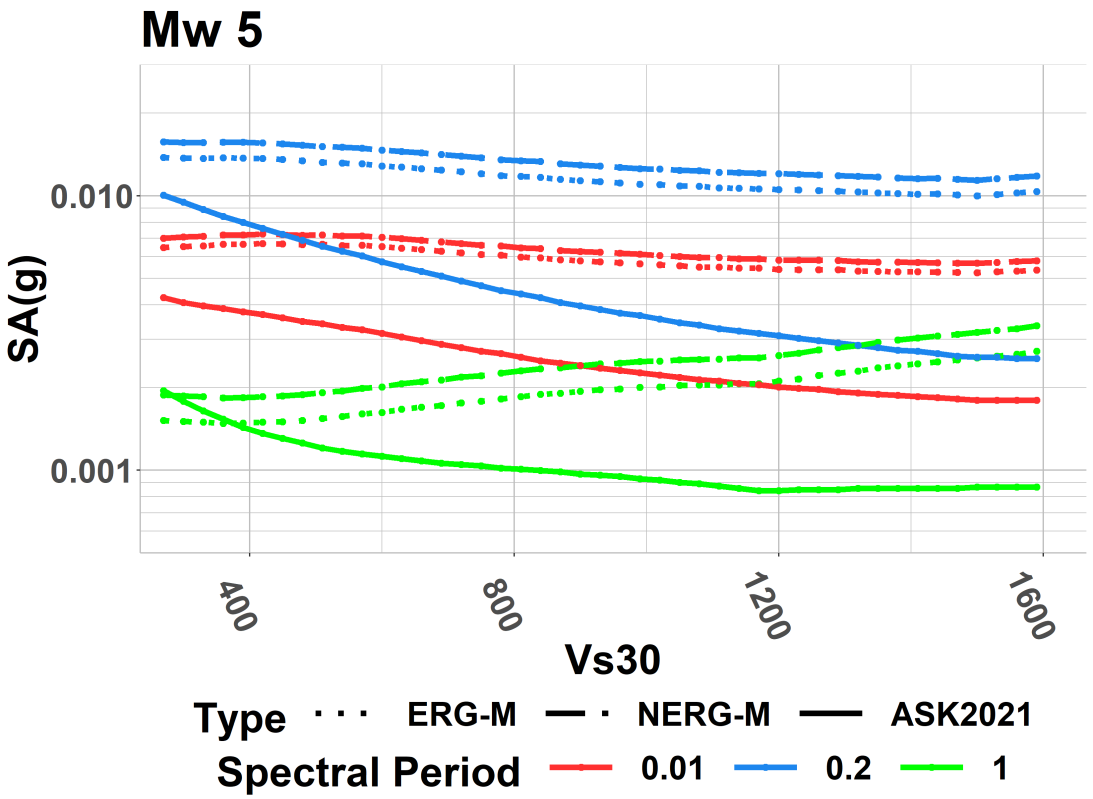

Figure 25: Mw 5.0

10 Spectral Correlation

We also explore the correlations between the event terms δB, station terms $\delta S2S$, and remaining residuals δWS_0 at different spectral periods. We calculate the empirical correlations between the terms, for the non-ergodic (NERG) and ergodic (ERG) models, using only event/station terms and records that are available at all periods. We compare the estimated correlations with the empirical calculations calculated from the respective terms of the ASK14 GMM, as well as the correlation model of Baker and Jayaram (2008) (BJ). Note that the BJ model is a correlation model for within-event residuals.

Figure 26 and Figure 27 show δB versus spectral period conditioned on PGA and 0.5 seconds, respectively. For the correlation conditioned on PGA, overall there is similar correlation between the difference models to 0.15 seconds. The NERG and ERG δ_B terms are more correlated at the longer periods than either the ASK or BJ correlations. Without further investigation it is not clear why these differences occur; it could be a magnitude effect, a regional

effect, or an effect inherent to PIE events.

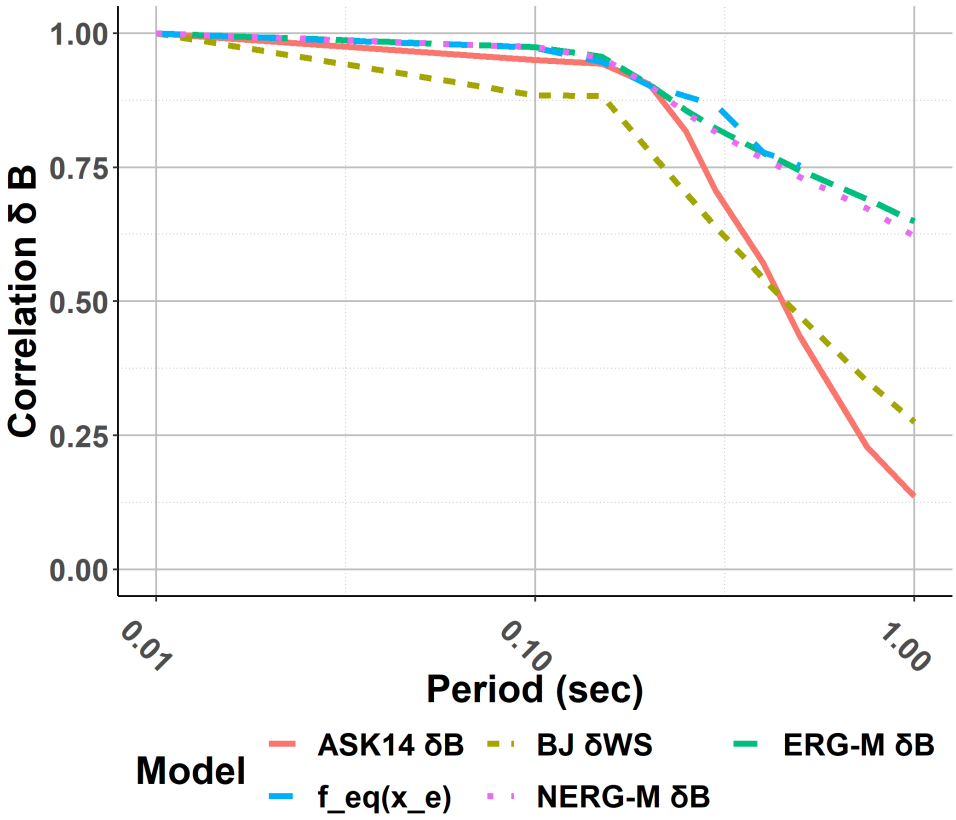

Figure 26: PGA

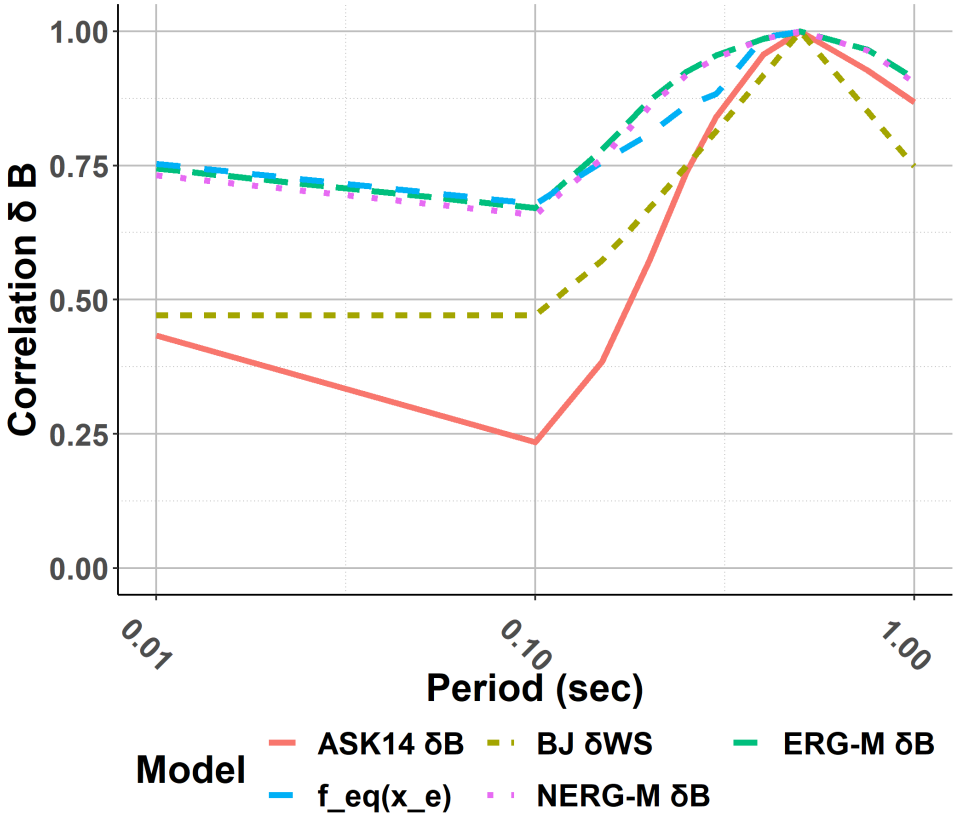

Figure 27: T=0.5 sec

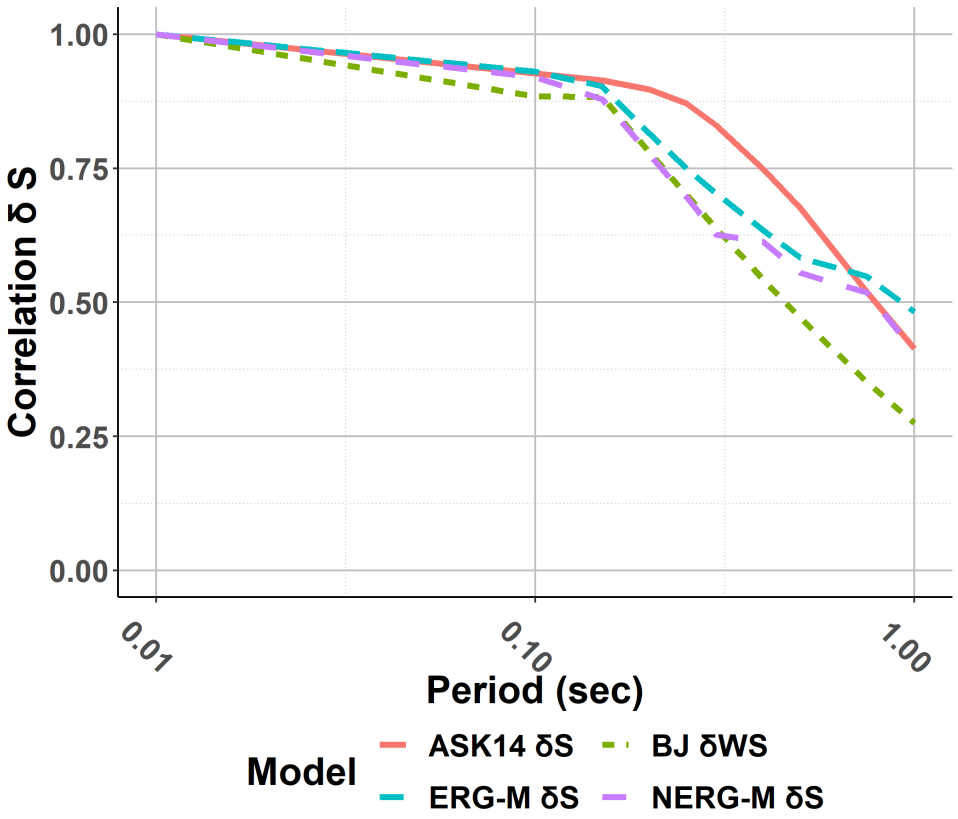

Figure 28: PGA

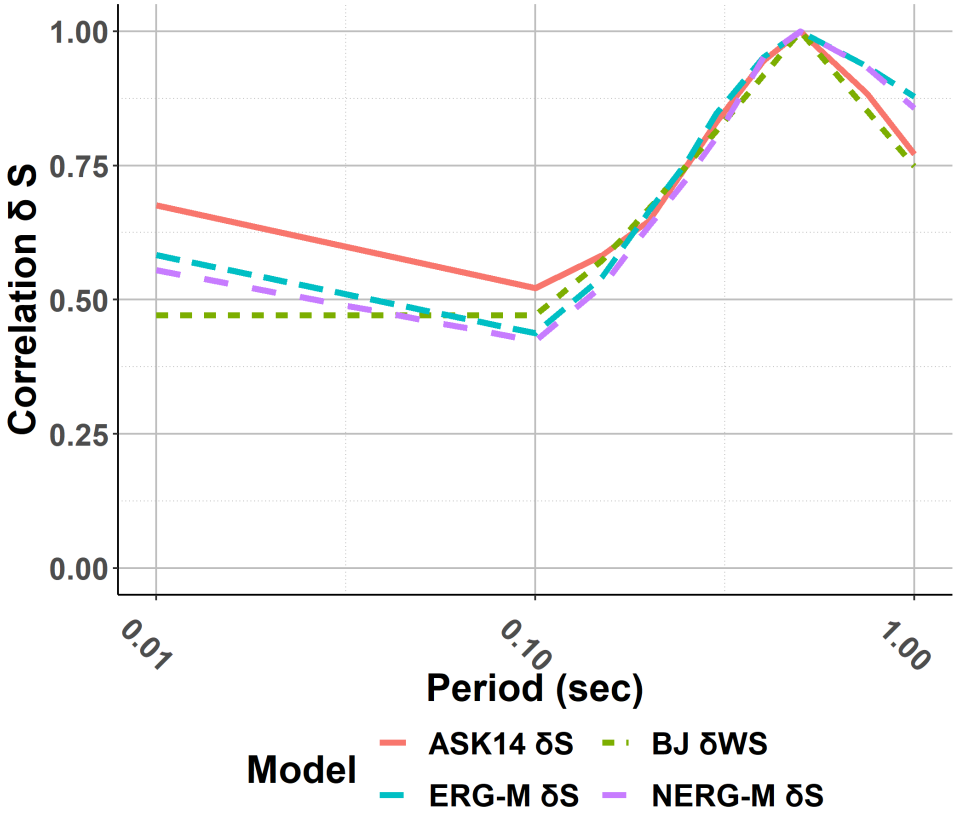

Figure 29: T=0.5 sec

The correlations for δS are shown in Figures 28 and 29; herre, the overall correlations are more consistent between the models. The last evaluation performed was for the correlation of $delta_{WS}$ which is shown in Figures 30 and 31 for PGA and 0.5 seconds, respectively. The correlations from the PNREG, ERG and BJ model are similar; whereas, ASK are similar only near the conditioning periods.

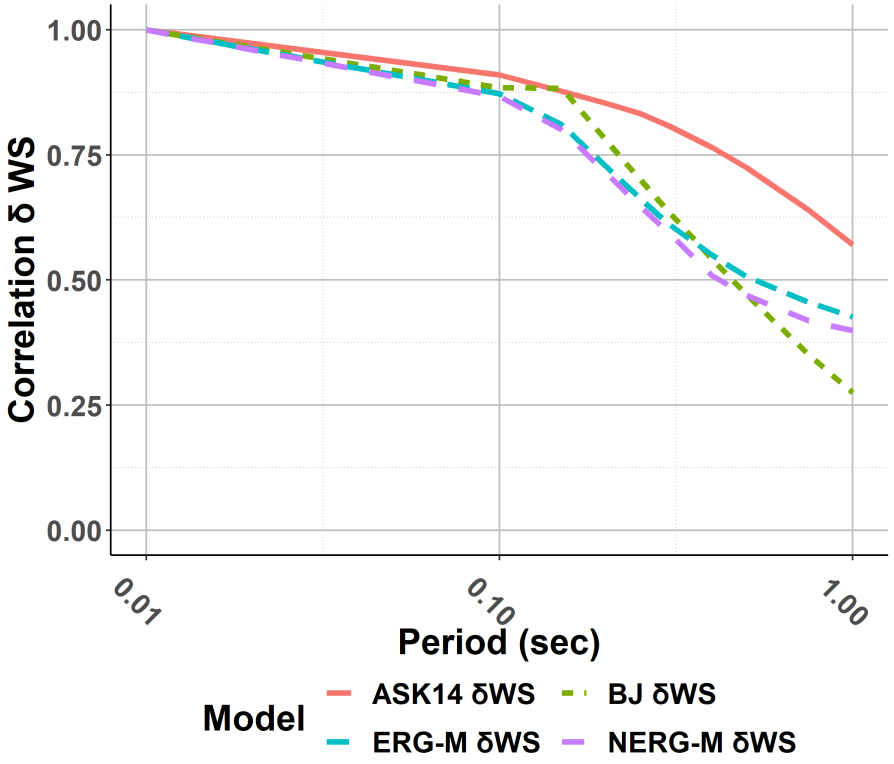

Figure 30: PGA

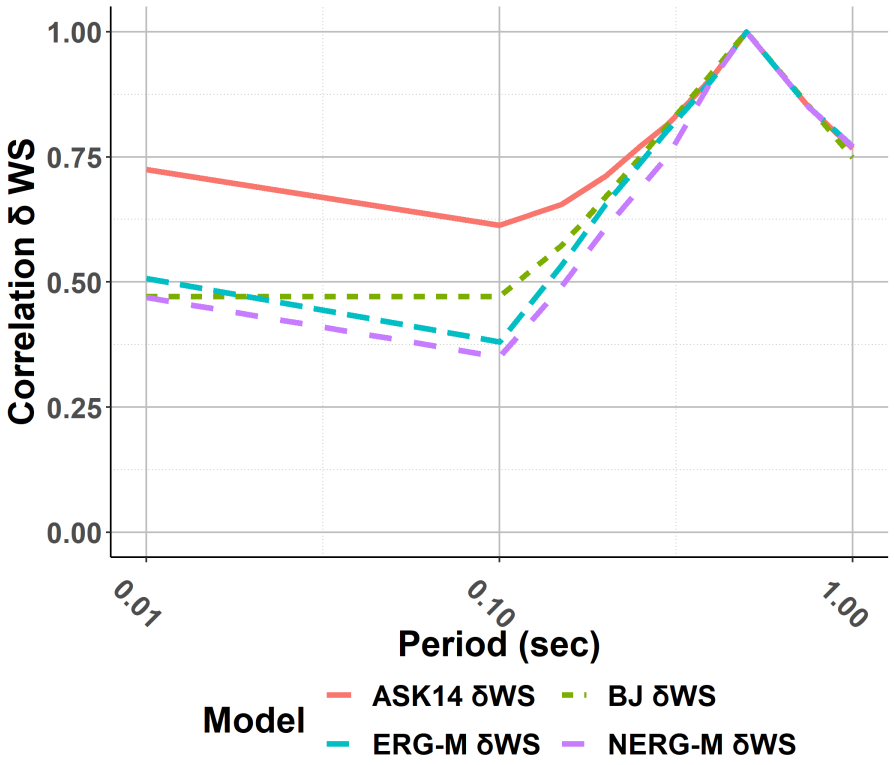

Figure 31: T=0.5 sec

11 Discussion

In total, apart from the random effects there were 10 parameters to estimate: 4 fixed effects (the intercept, the Moho bounce adjustment, the linear site scaling adjustment, the linear R-term), and six hyperparameters (ϕ_0, τ_0, $\phi_{S2S,0}$, the range and standard deviation of the systematic event constants, and the standard deviation of the cell-specific attenuation terms).

In the model building process, we tried different versions of the degree to which we could relax the ergodic assumption but were ultimately limited by the dataset in several ways. As mentioned earlier, we attempted in include spatially varying site term f_s; however, the separation distance between stations within the dataset could not resolve this term. Subsequently it was dropped from the model. The model was also limited by the number of records available at the different spectral periods. Generally, the model coefficients up to $T \leq 0.3$ seconds were well behaved, showing trends that were expected, which allowed all coefficients to be estimated. At $T > 03$ seconds the initial model coefficients were less behaved and several coefficients were constrained.

Further work on this model will look at addressing several items. The dataset bias between the magnitude correction and the ASK21 GMM was likely mapped into our GMM coefficients. The bias should be removed prior to use of the GMM. The Vs30 scaling in the GMM should also be addressed. Our Vs30 scaling at longer periods increases with increasing Vs30. This is physically implausible. Hence, the Vs30 scaling coefficient should be constrained to be less than the ASK21 Vs30 scaling coefficient, which would removed this undesired effect. The differences between the spectral correlation of our GMM to the ASK GMM should also be investigated further. We see differences in the correlations from our model (both ergodic and non-ergodic) and previously published models. In general, spectral correlations are quite stable across different regions and data sets, so it should be investigated whether this is inherit to he GMM formulation, or possibly PIE events.

As a supplement to this report, we provide an electronic copy of the GMM coefficients.

12 Acknowledgements

This research was funded by the USGS National Earthquake Hazards Reduction Program External Program through grant G18AP00076.

References

Abrahamson, N., Chiou, B., and Kuehn, N. (2021). "Modification of the NGA West 2 GMMs for Application to Induced Earthquakes." (0).

Abrahamson, N., Kuehn, N., Walling, M., and Landwehr, N. (2019). "Probabilistic Seismic Hazard Analysis in California Using Nonergodic Ground Motion Models." *Bulletin of the Seismological Society of America*, 109(4), 1235–1249.

Abrahamson, N. A., Silva, W. J., and Kamai, R. (2014). "Summary of the ASK14 Ground Motion Relation for Active Crustal Regions." *Earthquake Spectra*, 30(3), 1025–1055.

Anderson, J. G. and Brune, J. N. (1999). "Probabilistic Seismic Hazard Analysis without the Ergodic Assumption." *Seismological Research Letters*, 70(1), 19–28.

Atkinson, G. M. (2006). "Single-Station Sigma." *Bulletin of the Seismological Society of America*, 96(2), 446–455.

Atkinson, G. M. and Assatourians, K. (2015). "Implementation and Validation of EXSIM (A Stochastic Finite-Fault Ground-Motion Simulation Algorithm) on the SCEC Broadband Platform." *Seismological Research Letters*, 86(1), 48–60.

Atkinson, G. M. and Assatourians, K. (2017). "Are ground-motion models derived from natural events applicable to the estimation of expected motions for induced earthquakes?." *Seismological Research Letters*, 88(2), 430–441.

Bachl, F. E., Lindgren, F., Borchers, D. L., and Illian, J. B. (2019). "inlabru: an R package for Bayesian spatial modelling from ecological survey data." *Methods in Ecology and Evolution*, 10(6), 760–766.

Baker, J. W. and Jayaram, N. (2008). "Correlation of spectral acceleration values from NGA ground motion models." *Earthquake Spectra*, 24(1), 299–317.

Bakka, H., Rue, H., Fuglstad, G.-A., Riebler, A., Bolin, D., Illian, J., Krainski, E., Simpson, D., and Lindgren, F. (2018). "Spatial modeling with R-INLA: A review." *Wiley Interdisciplinary Reviews: Computational Statistics*, 10(6), e1443.

Bayliss, K., Naylor, M., Illian, J., and Main, I. G. (2020). "Data-Driven Optimization of Seismicity Models Using Diverse Data Sets: Generation, Evaluation, and Ranking Using Inlabru." *Journal of Geophysical Research: Solid Earth*, 125(11).

Bivand, R. S., Gómez-Rubio, V., and Rue, H. (2015). "Spatial Data Analysis with R - INLA with Some Extensions." *Journal of Statistical Software*, 63(20), 1–31.

Boore, D. M. (2010). "Orientation-Independent, Nongeometric-Mean Measures of Seismic Intensity from Two Horizontal Components of Motion." *Bulletin of the Seismological Society of America*, 100(4), 1830–1835.

Bussas, M., Sawade, C., Kühn, N., Scheffer, T., and Landwehr, N. (2017). "Varying-coefficient models for geospatial transfer learning." *Machine Learning*, 106(9-10), 1419–1440.

Caramenti, L., Menafoglio, A., Sgobba, S., and Lanzano, G. (2020). "Multi-Source Geographically Weighted Regression for Regionalized Ground-Motion Models." *Report no.*, <https://mox.polimi.it/publication-results/?id=917

D'Angelo, N., Abbruzzo, A., and Adelfio, G. (2020). "Spatial Bayesian Hierarchical Modelling with Integrated Nested Laplace Approximation." *arXiv*, 1–22.

Dawood, H. M. and Rodriguez-Marek, A. (2013). "A Method for Including Path Effects in Ground-Motion Prediction Equations: An Example Using the Mw 9.0 Tohoku Earthquake Aftershocks." *Bulletin of the Seismological Society of America*, 103(2B), 1360–1372.

Franco-Villoria, M., Ventrucci, M., and Rue, H. (2019). "A unified view on Bayesian varying coefficient models." *Electronic Journal of Statistics*, 13(2), 5334–5359.

Fuglstad, G.-A., Simpson, D., Lindgren, F., and Rue, H. (2019). "Constructing Priors that Penalize the Complexity of Gaussian Random Fields." *Journal of the American Statistical Association*, 114(525), 445–452.

Gelfand, A. E., Kim, H.-J., Sirmans, C. F., and Banerjee, S. (2003). "Spatial Modeling With Spatially Varying Coefficient Processes." *Journal of the American Statistical Association*, 98(462), 387–396.

Gómez-Rubio, V. (2020). *Bayesian inference with INLA*. Chapman and Hall/CRC, Boca Raton, FL.

Goulet, C., Abrahamson, N., Kuehn, N., Atik, L. A., Youngs, R., Graves, R., and Atkinson, G. (2018). "Central and Eastern North America Ground-Motion Characterization - NGA-East Final Report." *Report no.*, Pacific Earthquake Engineering Research Center.

Goulet, C. A., Bozorgnia, Y., Kuehn, N., Al Atik, L., Youngs, R. R., Graves, R. W., and Atkinson, G. M. (2021). "NGA-East Ground-Motion Characterization model part I: Summary of products and model development." *Earthquake Spectra*, 37(1_suppl), 1231–1282.

Gregor, N. (2018). "Flat file for induced events, dated Mar 30, 2018." *Data file prepared by BCHydro*, (0).

Krainski, E., Gómez-Rubio, V., Bakka, H., Lenzi, A., Castro-Camilo, D., Simpson, D., Lindgren, F. K., and Rue, H. (2019). *Advanced Spatial Modeling with Stochastic Partial Differential Equations Using R and INLA*. Chapman and Hall/CRC, Boca-Raton, FL.

Kuehn, N. (2021a). "A Comparison of Nonergodic Ground-Motion Models based on Geographically Weighted Regression and the Integrated Nested Laplace Approximation." *Engrxiv*.

Kuehn, N. (2021b). "A Primer for using INLA to Estimate Ground-Motion Models." *Engrxiv*, 1–30.

Kuehn, N. (2021c). "Comparison of Bayesian Varying Coefficient Models for the Development of Nonergodic Ground-Motion Models." *Engrxiv*, 1–25.

Kuehn, N. M. and Abrahamson, N. A. (2020). "Spatial correlations of ground motion for nonergodic seismic hazard analysis." *Earthquake Engineering & Structural Dynamics*, 49(1), 4–23.

Kuehn, N. M., Abrahamson, N. A., and Walling, M. A. (2019). "Incorporating Nonergodic Path Effects into the NGA-West2 Ground-Motion Prediction Equations." *Bulletin of the Seismological Society of America*, 109(2), 575–585.

Landwehr, N., Kuehn, N. M., Scheffer, T., and Abrahamson, N. (2016). "A Nonergodic Ground-Motion Model for California with Spatially Varying Coefficients." *Bulletin of the Seismological Society of America*, 106(6), 2574–2583.

Lanzano, G., Sgobba, S., Caramenti, L., and Menafoglio, A. (2021). "Ground-Motion Model for Crustal Events in Italy by Applying the Multisource Geographically Weighted Regression (MS-GWR) Method." *Bulletin of the Seismological Society of America*, 1–17.

Lavrentiadis, G., Abrahamson, N. A., and Kuehn, N. M. (2021). *A Non-ergodic Effective Amplitude Ground-Motion Model for California*. Number 0123456789. Springer Netherlands, <http://arxiv.org/abs/2106.07834>.

Lezama-Ochoa, N., Pennino, M. G., Hall, M. A., Lopez, J., and Murua, H. (2020). "Using a Bayesian modelling approach (INLA-SPDE) to predict the occurrence of the Spinetail Devil Ray (Mobular mobular)." *Scientific Reports*, 10(1), 1–11.

Lindgren, F. and Rue, H. (2015). "Bayesian Spatial Modelling with R - INLA." *Journal of Statistical Software*, 63(19), 1–25.

Lindgren, F., Rue, H., and Lindström, J. (2011). "An explicit link between gaussian fields and gaussian markov random fields: The stochastic partial differential equation approach." *Journal of the Royal Statistical Society. Series B: Statistical Methodology*, 73(4), 423–498.

Martino, S. and Riebler, A. (2020). " Integrated Nested Laplace Approximations (INLA) ." *Wiley StatsRef: Statistics Reference Online*, 1–19.

Moraga, P. (2019). *Geospatial Health Data: Modeling and Visualization with R-INLA and Shiny.* Chapman and Hall/CRC, <https://www.paulamoraga.com/book-geospatial/index.html>.

R Core Team (2021). "R: A Language and Environment for Statistical Computing, <https://www.r-project.org/>.

Rasmussen, C. E. and Williams, C. K. I. (2006). *Gaussian Processes for Machine Learning.* MIT Press, Cambridge, <http://www.gaussianprocess.org/gpml/>.

Rennolet, S. B., Moschetti, M. P., Thompson, E. M., and Yeck, W. L. (2018). "A Flatfile of Ground Motion Intensity Measurements from Induced Earthquakes in Oklahoma and Kansas." *Earthquake Spectra*, 34(1), 1–20.

Rodriguez-Marek, A., Montalva, G. A., Cotton, F., and Bonilla, F. (2011). "Analysis of Single-Station Standard Deviation Using the KiK-net Data." *Bulletin of the Seismological Society of America*, 101(3), 1242–1258.

Rodriguez-Marek, A., Rathje, E. M., Bommer, J. J., Scherbaum, F., and Stafford, P. J. (2014). "Application of single-station sigma and site-response characterization in a probabilistic seismic-hazard analysis for a new nuclear site." *Bulletin of the Seismological Society of America*, 104(4), 1601–1619.

Rue, H., Martino, S., and Chopin, N. (2009). "Approximate Bayesian inference for latent Gaussian models by using integrated nested Laplace approximations." *Journal of the Royal Statistical Society: Series B (Statistical Methodology)*, 71(2), 319–392.

Rue, H., Riebler, A., Sørbye, S. H., Illian, J. B., Simpson, D. P., and Lindgren, F. K. (2017). "Bayesian Computing with INLA: A Review." *Annual Review of Statistics and Its Application*, 4(1), 395–421.

Schrödle, B. and Held, L. (2011). "A primer on disease mapping and ecological regression using INLA." *Computational Statistics*, 26(2), 241–258.

Simpson, D., Lindgren, F., and Rue, H. (2012). "In order to make spatial statistics computationally feasible, we need to forget about the covariance function." *Environmetrics*, 23(1), 65–74.

Simpson, D., Rue, H., Riebler, A., Martins, T. G., and Sørbye, S. H. (2017). "Penalising Model Component Complexity: A Principled, Practical Approach to Constructing Priors." *Statistical Science*, 32(1), 1–28.

Stafford, P. J. (2014). "Crossed and Nested Mixed-Effects Approaches for Enhanced Model Development and Removal of the Ergodic Assumption in Empirical Ground-Motion Models." *Bulletin of the Seismological Society of America*, 104(2), 702–719.

Sung, C.-H., Abrahamson, N. A., Kuehn, N. M., Traversa, P., and Zentner, I. (2021). "A non-ergodic ground-motion model of fourier amplitude spectra for france." *submitted to Bulletin of Earthquake Engineering*.

Trugman, D. T. and Shearer, P. M. (2018). "Strong Correlation between Stress Drop and Peak Ground Acceleration for Recent M 1–4 Earthquakes in the San Francisco Bay Area." *Bulletin of the Seismological Society of America*, 108(2), 929–945.

Vilela, R., Burger, C., Diederichs, A., Bachl, F. E., Szostek, L., Freund, A., Braasch, A., Bellebaum, J., Beckers, B., Piper, W., and Nehls, G. (2021). "Use of an INLA Latent Gaussian Modeling Approach to Assess Bird Population Changes Due to the Development of Offshore Wind Farms." *Frontiers in Marine Science*, 8(July), 1–11.

Villani, M. and Abrahamson, N. A. (2015). "Repeatable Site and Path Effects on the Ground-Motion Sigma Based on Empirical Data from Southern California and Simulated Waveforms from the CyberShake Platform." *Bulletin of the Seismological Society of America*, 105(5), 2681–2695.

Walling, M. and Abrahamson, N. A. (2012). "Non-Ergodic Probabilistic Seismic Hazard Analyses." *15th World Conference on Earthquake Engineering (15WCEE)*.

Wilson, B. (2020). "Evaluating the INLA-SPDE approach for Bayesian modeling of earthquake damages from geolocated cluster data." *EarthArXiv*.

Yenier, E. and Atkinson, G. M. (2015). "Regionally adjustable generic ground-motion prediction equation based on equivalent point-source simulations: Application to central and eastern North America." *Bulletin of the Seismological Society of America*, 105(4), 1989–2009.

Zhang, R., Czado, C., and Sigloch, K. (2016). "Bayesian spatial modelling for high dimensional seismic inverse problems." *Journal of the Royal Statistical Society: Series C (Applied Statistics)*, 65(2), 187–213.